



HAL
open science

Millennial-scale deglaciation across the European Alps at the transition between the Younger Dryas and the Early Holocene - evidence from a new cosmogenic nuclide chronology

Marie Protin, Irene Schimmelpfennig, Jean-louis Mugnier, Jean-françois Buoncristiani, Melaine Le Roy, Benjamin Pohl, Luc Moreau

► To cite this version:

Marie Protin, Irene Schimmelpfennig, Jean-louis Mugnier, Jean-françois Buoncristiani, Melaine Le Roy, et al.. Millennial-scale deglaciation across the European Alps at the transition between the Younger Dryas and the Early Holocene - evidence from a new cosmogenic nuclide chronology. *Boreas*, 2021, 50 (3), pp.671-685. 10.1111/bor.12519 . hal-03290256v2

HAL Id: hal-03290256

<https://hal.science/hal-03290256v2>

Submitted on 13 Jan 2022

HAL is a multi-disciplinary open access archive for the deposit and dissemination of scientific research documents, whether they are published or not. The documents may come from teaching and research institutions in France or abroad, or from public or private research centers.

L'archive ouverte pluridisciplinaire **HAL**, est destinée au dépôt et à la diffusion de documents scientifiques de niveau recherche, publiés ou non, émanant des établissements d'enseignement et de recherche français ou étrangers, des laboratoires publics ou privés.

1
2
3 1 Millennial-scale deglaciation across the European Alps at the
4
5 2 transition between the Younger Dryas and the Early Holocene –
6
7 3 evidence from a new cosmogenic nuclide chronology
8
9 4

10
11
12 5 MARIE PROTIN, IRENE SCHIMMELPFENNIG, JEAN-LOUIS MUGNIER, JEAN-
13
14 6 FRANÇOIS BUONCRISTIANI, MELAINE LE ROY, BENJAMIN POHL, LUC MOREAU
15
16
17 7 AND ASTER TEAM
18

19 8
20
21 9 Protin, M., Schimmelpfennig, I., Mugnier, J.-L., Buoncristiani, J.-F., Le Roy, M., Pohl, B.,
22
23
24 10 Moreau, L. & ASTER Team: Millennial-scale deglaciation across the European Alps at the
25
26 11 transition between the Younger Dryas and the Early Holocene – evidence from a new
27
28 12 cosmogenic nuclide chronology. *Boreas*....
29
30
31 13

32
33 14 Reconstructing the spatial and temporal response of mountain glaciers to rapid climate change
34
35 15 in the past provides access to the effects of current climate change. Yet, the spatial and temporal
36
37 16 variability of past glacier fluctuations is not fully understood. In this study, we focus on the
38
39 17 timing of glacier fluctuations in the European Alps during the Younger Dryas/Early Holocene
40
41 18 (YD/EH) transition. In an effort to elucidate whether glacier fluctuations were synchronous
42
43 19 during this period, we present a new chronology of the Alpine Talèfre glacier, based on 14 new
44
45 20 ^{10}Be ages of moraines and roches moutonnées. The retreat of Talèfre glacier was initiated
46
47 21 during the mid-YD (~12.4 ka), then it experienced a gradual retreat punctuated by at least 3
48
49 22 oscillations until ~11 ka before shrinking substantially within its Little Ice Age limits (13th -
50
51 23 19th century). Comparison of our findings with published glacier chronologies in the Alpine
52
53 24 region highlights broadly synchronous behaviour of glaciers across the Alps between 12 and
54
55 25 10 ka. The coeval glacier fluctuations at a regional scale suggest that common regional climate
56
57 26 conditions had a major impact on Alpine glacier variations during the YD/EH transition. The
58
59 27 similarity of glacier behaviour and independent temperature records in both the Alpine region
60
60 28 and the northern high latitudes suggests a teleconnection between these regions, but differences

1
2
3
4 29 in the amplitude of the mean annual temperature signals relative to summer temperature
5 30 indicate pronounced changes in seasonality between the YD and the EH.
6
7 31

8
9 32 *Marie Protin (marie.protin@univ-lorraine.fr), Aix-Marseille Université, CNRS, IRD, INRA,*
10
11 33 *Coll France, CEREGE, Aix en Provence, France and Université de Lorraine, CNRS, CRPG,*
12
13 34 *F-54000 Nancy, France; Irene Schimmelpfennig and ASTER Team (Georges Aumaître, Didier*
14
15 35 *Bourlès, Karim Keddadouche), Aix-Marseille Université, CNRS, IRD, INRA, Coll France,*
16
17 36 *CEREGE, Aix en Provence, France; Jean-Louis Mugnier, Université Grenoble Alpes,*
18
19 37 *Université Savoie Mont Blanc, CNRS, ISTERre, 73000 Chambéry, France; Jean-François*
20
21 38 *Buoncrisiani and Benjamin Pohl, Biogéosciences, UMR 6282 CNRS, Université Bourgogne*
22
23 39 *Franche-Comté, 6 Boulevard Gabriel, 21000 Dijon, France; Melaine Le Roy, University of*
24
25 40 *Geneva, Institute for Environmental Sciences, Climate Change Impacts and Risks in the*
26
27 41 *Anthropocene (C-CIA), CH-1205 Geneva, Switzerland and Université Grenoble Alpes,*
28
29 42 *Université Savoie Mont Blanc, CNRS, EDYTEM, 73000 Chambéry, France; Luc Moreau,*
30
31 43 *Université Grenoble Alpes, Université Savoie Mont Blanc, CNRS, EDYTEM, 73000 Chambéry,*
32
33 44 *France ; received 23rd November 2020, accepted 11th February 2021.*
34
35
36
37
38
39
40

41 46 Mountain glaciers are recognized as sensitive recorders of climate variability, and their
42
43 47 fluctuations mainly depend on variations of both temperature during the melt season and snow
44
45 48 precipitation (Oerlemans 2005; Roe *et al.* 2017). In the case of Alpine glaciers, their recent
46
47 49 evolution is controlled by large-scale climate variations moderated by local specific factors
48
49 50 (Rabatel *et al.* 2013; Vincent *et al.* 2017). In the light of current climate evolution and rapid
50
51 51 retreat of glaciers worldwide, it is important to improve our understanding of the sensitivity of
52
53 52 glaciers to rapid climate changes in the past, such as those during the Younger Dryas/Early
54
55 53 Holocene (YD/EH) transition (between ~12 and 10 ka). Therefore, the impact of large-scale
56
57
58
59
60

1
2
3 54 climate variations versus local climate and site-specific factors has to be better assessed by
4
5 55 constraining past glacial chronologies.
6

7
8 56 Moraines and roches moutonnées represent clear geomorphic markers of past glacier
9
10 57 extents. Studying and dating them is a valuable approach for constraining former glacier
11
12 58 behaviour, establishing glacier chronologies and investigating the related climate changes. Due
13
14 59 to the lack of direct dating methods, the traditional chronology of glacier advances (“stadials”)
15
16 60 in the Alps during the period of Lateglacial and EH deglaciation is mainly based on comparative
17
18 61 studies of moraine stratigraphies and morphologies and on the variation of the equilibrium line
19
20 62 altitude (ELA) (e.g. Maisch 1981). Temporal correlations of these stadials with palaeoclimatic
21
22 63 periods were broadly confirmed by the pioneering cosmogenic nuclide studies at a few Alpine
23
24 64 sites (see reviews in Ivy-Ochs *et al.* 2006 and Ivy-Ochs 2015). For instance, the Egesen stadal
25
26 65 moraines are assigned to the Younger Dryas (from 12.9 to 11.7 ka; Rasmussen *et al.* 2006), and
27
28 66 are associated with an ELA depression of 250-350 m relative to the Little Ice Age (LIA) (Ivy-
29
30 67 Ochs 2015). The Kartell stadal moraines are assigned to the Preboreal cold period (11.4 – 11.3
31
32 68 ka; Kobashi *et al.* 2008) with an ELA depression of 120 m (Ivy-Ochs 2015). However, recent
33
34 69 studies showed that correlating moraines from different Alpine valleys solely based on the
35
36 70 above-mentioned comparative criteria is unreliable, highlighting the need for direct moraine
37
38 71 dating with cosmogenic nuclides when comparing moraines from various sites (e.g. Reitner *et*
39
40 72 *al.* 2016; Boxleitner *et al.* 2019).
41
42
43
44
45

46
47 73 Over the past few years, parameters for the calculations of cosmic ray exposure ages
48
49 74 were refined (e.g. Balco *et al.* 2008, 2009; Young *et al.* 2013; Borchers *et al.* 2016; Balco 2017;
50
51 75 Martin *et al.* 2017) and an increasing number of cosmogenic nuclide dating studies from the
52
53 76 Alps have been published, providing evidence of multiple glacier fluctuations during the
54
55 77 Lateglacial and the EH (e.g. Schindelwig *et al.* 2012; Moran *et al.* 2016a, b; Baroni *et al.* 2017).
56
57 78 Attempts of identifying temporal or spatial trends in Alpine glacier behaviour during the
58
59
60

1
2
3 79 Lateglacial and EH have been made in earlier studies (Schimmelpfennig *et al.* 2014; Chenet *et*
4
5 80 *al.* 2016; Braumann *et al.* 2020). Although age uncertainties are generally too large to infer
6
7 81 clear trends, an abrupt glacier recession is not documented in the Alps at the very sharp
8
9 82 transition between YD and Holocene that is observed in Greenland ice cores with a ~ 10 °C
10
11 83 warming in less than one hundred years.

12
13
14 84 Rather, previous studies suggested that EH glacier stillstands or advances in the Alps
15
16 85 could be a response to abrupt cold spells observed in Greenland ice cores (e.g. Ivy-Ochs *et al.*,
17
18 86 2009; Schindelwig *et al.* 2012; Schimmelpfennig *et al.* 2012, 2014), such as the Preboreal
19
20 87 Oscillation or a cold event notable at ~ 10.9 ka (Rasmussen *et al.* 2006; Vinther *et al.* 2006).

21
22
23 88 In the Western Alps, glacier chronologies from Lateglacial and EH have for a long time
24
25 89 been very scarce, but recent robust records and additional data from the French Alps will now
26
27 90 provide the opportunity to use the Alpine data set as a whole for a regional analysis (e.g. Cossart
28
29 91 *et al.* 2012; Chenet *et al.* 2016; Hofmann 2018; Protin *et al.* 2019; Schimmelpfennig *et al.*
30
31 92 2019). The chronological investigation of these moraine chronologies could lead to a better
32
33 93 understanding of the large-scale palaeoclimatic conditions during a period for which proxy and
34
35 94 model data still show diverging temperature trends in both mid- and high latitudes: coupled
36
37 95 ocean-atmosphere climate models (e.g. Buizert *et al.* 2014) failed to reproduce the abrupt
38
39 96 warming at the end of the YD found in North Atlantic and Greenland ice cores (e.g. Rasmussen
40
41 97 *et al.* 2006; Shakun *et al.* 2015), whereas continental temperature reconstructions based on
42
43 98 biological proxies either fit with this drastic warming (chironomid records in Heiri *et al.* 2015)
44
45 99 or indicate a much more gradual warming (e.g. pollen records in Marsicek *et al.* 2018 and
46
47 100 glacier chronologies in Rainsley *et al.* 2018, and Young *et al.* 2020).

48
49
50 101 In this study, we provide a new glacier chronology in the French Alps by analyzing the
51
52 102 Talèfre glacier patterns during the deglaciation of the “Jardin de Talèfre”, one of the highest
53
54 103 moraine sites in the Alps (close to 3000 m a.s.l.), where a set of moraines is deposited above
55
56
57
58
59
60

1
2
3 104 roches moutonnées. We present new *in-situ* cosmogenic beryllium-10 (^{10}Be) ages of moraines
4
5 105 and roches moutonnées for this area and compare these new data with published ^{10}Be glacial
6
7 106 chronologies from elsewhere in the European Alps, selected for their quality (e.g. number of
8
9 107 samples, dispersion of the ages) and re-calculated using uniform methods. Building on this
10
11 108 regional compilation, we evaluate (i) the possibility of a regional synchronicity of glacier
12
13 109 fluctuations during the multi-millennia period of the end of the YD and the beginning of the
14
15 110 Holocene (hereafter YD/EH transition), (ii) the impact of large-scale climate variations on
16
17 111 glacier patterns versus site-specific factors, (iii) the underlying climatic drivers in a regional
18
19 112 scale and their potential link with the high-latitudes, and (iv) the climatic significance of the
20
21 113 small fluctuation range of glacier extent between the YD and EH in the light of the significant
22
23 114 and abrupt climate change recorded in independent proxy records.
24
25
26
27
28
29
30

31 116 Study site

32
33 117
34
35
36 118 Talèfre glacier ($45^{\circ}54'\text{N}$, $6^{\circ}59'\text{E}$) is a cirque glacier located in the French part of the Mont-
37
38 119 Blanc massif and was a major tributary of Mer de Glace glacier, the largest glacier in the Mont-
39
40 120 Blanc massif (Fig. 1). To the north is located the Argentièrre glacier, the second largest glacier
41
42 121 in the Mont-Blanc massif (Fig. 1). In 2008, Talèfre glacier covered an area of $\sim 8 \text{ km}^2$ with a
43
44 122 maximum length of 4.5 km and altitude spanning 2473 to 3743 m a.s.l. (Gardent 2014). The
45
46 123 ELA of Talèfre glacier for the period 1984-2010 was estimated to $\sim 3000 \text{ m a.s.l.}$ (Rabatel *et al.*
47
48 124 2013). Next to Argentièrre glacier, the mean annual temperature and precipitation for the time
49
50 125 period 1979-2002 are estimated at 1.8°C and 1783 mm at $\sim 2000 \text{ m a.s.l.}$ (Joly *et al.* 2018; D.
51
52 126 Joly pers. comm. 2018). The catchment of Talèfre glacier is bordered by granite rocks of late
53
54 127 Hercynian age ($\sim 300 \text{ Ma}$; Bussy *et al.* 2000).
55
56
57
58
59
60

1
2
3 128 During the YD, Talèfre glacier was connected to Mer de Glace, which at that time
4
5 129 occupied the Arve Valley with a front located westward of the left boundary of Fig. 1
6
7
8 130 (Prud'homme *et al.* 2020). During the last LIA advance in the 19th century, Talèfre glacier was
9
10 131 confluent with Leschaux glacier, which further downvalley joins Tacul glacier to form Mer de
11
12 132 Glace (Fig. 1). Since ~1950 the Talèfre and Leschaux glaciers have not been coalescing
13
14
15 133 (Gardent 2014).

16
17 134 A notable feature of Talèfre glacier is the presence of a triangle-shaped rock islet at its
18
19 135 center, named “Jardin de Talèfre” (i.e. Talèfre garden). This islet is bounded by moraines (Fig.
20
21 136 2), that span 2640 to 3040 m a.s.l. (Jordan 2010). Because of its remoteness, this area has not
22
23
24 137 been disturbed by human activity. According to the French État-Major maps (surveyed in 1820-
25
26 138 1866) and first available photographs made by August-Rosalie Bisson in 1862 the “Jardin de
27
28 139 Talèfre” was not ice-covered during the last LIA maximum (de Decker Heftler 2002).

30
31 140

32 33 141 Methodology

34 35 142 *Moraine mapping*

36
37
38 143

39
40 144 Several so-far undated moraine ridges preserved on the islet were studied and represented in
41
42 145 the geomorphological map of Fig. 3. The mapping was conducted through field work and
43
44
45 146 interpretation of aerial images from the year 2015 (French national institute of geographic and
46
47 147 forest information - IGN, 50 cm resolution).

48
49
50 148

51 52 149 *Sample collection*

53
54 150

55
56 151 Fourteen samples were collected in the “Jardin de Talèfre”, 2 from smoothed bedrock surfaces
57
58
59 152 resulting from glacial erosion and 12 from moraine boulders (Fig. 3). Bedrock samples were
60

1
2
3 153 taken from the surface of the rocky islet, and attention was paid to avoid the possibility of cover
4
5 154 by snow or vegetation and significant erosion by choosing sloping spots with glacial
6
7 155 morphologies (Fig. 2C). Both surfaces were covered by lichen. Moraine boulder samples were
8
9
10 156 taken from the top of the boulders, which were embedded in the crest or slope of the targeted
11
12 157 moraines (Fig. 2D). If we assume uninterrupted surface exposure, the bedrock exposure ages
13
14 158 indicate when the “Jardin de Talèfre” became ice-free for the last time, while the boulder
15
16 159 exposure ages represent the timing of the glacier culmination and moraine stabilization (for
17
18 160 detailed discussion see section “Oscillation of Talèfre glacier since the Younger Dryas”).
19
20 161 Samples were collected using a chisel, a hammer and a cordless angle grinder, and topographic
21
22 162 shielding was evaluated in the field using a clinometer.
23
24
25

26 163

28 164 *Laboratory procedures*

30 165

32
33 166 All samples were processed at CEREGE (Aix-en-Provence, France). Samples were crushed and
34
35 167 sieved to collect the 250-500 μm fraction. Quartz was first concentrated by magnetic separation
36
37 168 and then isolated by successive leaching in a $\text{H}_2\text{SiF}_6/\text{HCl}$ mixture or by froth flotation when the
38
39 169 mineralogy allowed it. The obtained quartz fraction was leached at least two times in a 5% HF
40
41 170 - 5% HNO_3 solution, followed by 24h in ultra-sonic baths in a 1% HF - 1% HNO_3 solution in
42
43 171 order to remove any remaining feldspars and to clean the grains from atmospheric ^{10}Be . Purified
44
45 172 quartz was completely dissolved in concentrated HF after addition of ~ 0.1 g of an in-house ^9Be
46
47 173 carrier solution (3025 ± 9 ppm; Merchel *et al.* 2008). Beryllium was extracted by successive
48
49 174 alkaline precipitations of $\text{Be}(\text{OH})_2$ alternated with separation on anion and cation columns.
50
51 175 Samples were then oxidized at 700 $^\circ\text{C}$ for one hour and the final BeO mixed with Nb powder
52
53 176 and loaded into nickel cathodes. Measurements of the $^{10}\text{Be}/^9\text{Be}$ ratios by accelerator mass
54
55 177 spectrometry (AMS) were conducted at the French national AMS facility ASTER (Arnold *et*
56
57
58
59
60

1
2
3 178 *al.* 2010). Samples were calibrated against in-house standard STD-11 with a $^{10}\text{Be}/^9\text{Be}$ ratio of
4
5 179 $(1.191\pm 0.013) \times 10^{-11}$ (Braucher *et al.* 2015) and a ^{10}Be half-life of $(1.387\pm 0.0012) \times 10^6$ years
6
7 180 (Chmeleff *et al.* 2010; Korschinek *et al.* 2010). Analytical uncertainties combine ASTER
8
9 181 counting statistics and stability ($\sim 5\%$; Arnold *et al.* 2010) and machine blank correction. The
10
11 182 number of atoms ^{10}Be in the samples calculated from the corresponding $^{10}\text{Be}/^9\text{Be}$ ratios was
12
13 183 then corrected from that of the chemical blanks, which had $^{10}\text{Be}/^9\text{Be}$ ratios of $(3.38\pm 0.49) \times 10^{-15}$
14
15 184 and $(3.48\pm 0.50) \times 10^{-15}$ (Table 1).
16
17
18
19
20
21

185

22 186 *Age calculations*23
24 187

25
26 188 Surface exposure ages of the here presented new data were computed with the CREp online
27
28 189 calculator (Martin *et al.* 2017) using the Lal-Stone time corrected scaling scheme Lm, the
29
30 190 ERA40 atmospheric reanalyses and the Atmospheric ^{10}Be -based VDM for geomagnetic
31
32 191 database (see Martin *et al.* 2017 and references therein). We applied the production rate of
33
34 192 4.10 ± 0.10 atoms $^{10}\text{Be} \text{ g}^{-1} \text{ a}^{-1}$ established by Claude *et al.* (2014) as it is the only regional ^{10}Be
35
36 193 production rate available for Alpine sites and it is identical to the global ^{10}Be production rate
37
38 194 resulting from the ICE-D database linked to CREp (4.11 ± 0.19 atoms $^{10}\text{Be} \text{ g}^{-1} \text{ a}^{-1}$). The two other
39
40 195 production rates often used for studies in the Alps, i.e. the northeast North America “NENA”
41
42 196 production rate (Balco *et al.* 2009) and the “Arctic” production rate (Young *et al.* 2013), which
43
44 197 is almost identical with the recent Scotland production rate (Putnam *et al.* 2019), would lead to
45
46 198 ages older by less than 2% and 1%, respectively. For easy comparison, we present in Table 1
47
48 199 the exposure ages calculated with both the regional production rate and the “Arctic” production
49
50 200 rate. We did not apply a correction for snow shielding, as we do not have sufficient quantitative
51
52 201 data on snowfall during the Holocene, and all sampled surfaces are in wind-exposed locations.
53
54 202 We did not correct for potential erosion, as we were careful to sample surfaces with least
55
56
57
58
59
60

1
2
3 203 possible erosion. Applying a correction for considerable snow cover assuming 50 cm of snow
4
5 204 for six months (Chenet *et al.* 2016) would lead to ages older by 6% to 8%. Applying a correction
6
7 205 for erosion corresponding to an erosion rate of 1 mm ka⁻¹ (André 2002) would result in ages
8
9 206 older by less than 1%.

10
11
12 207 For the regional comparison of glacier records, previously published data from 18 study
13
14 208 sites (see references in Fig. 6) were homogenized by re-calculating the individual and mean
15
16 209 ages using the same procedures as above (Table S1). Boulders identified as outliers in the
17
18 210 original studies were kept as outliers. Applying the χ^2 test (2σ) by Ward & Wilson (1978),
19
20 211 moraine age populations were tested for outliers, which were also discarded as indicated in
21
22 212 Table S1. Exceptions were made for the moraine M7a from the Rougnoux valley, M2 from
23
24 213 Falgin cirque and the lower moraine from Steingletscher, where all boulders (not identified as
25
26 214 outliers by authors) were kept for the mean age calculation even if they statistically mismatch,
27
28 215 as we do not have any argument for discarding a specific sample from the age population. At
29
30 216 the Rougnoux valley site, several moraine mean ages do not agree with the stratigraphic order
31
32 217 (M8-9, M7b, M4-5 and M6b) but these ages do not statistically differ; therefore, we choose to
33
34 218 include them all in the comparison. We eliminated from the comparison the moraine ages that
35
36 219 are based on only one sample and that have standard deviations >10% to make the comparison
37
38 220 as accurate as possible. Once this selection made, only the sites with at least one moraine of
39
40 221 Holocene age (<11.7 ka) were kept for the comparison in order to exclude sites with moraines
41
42 222 that exclusively correspond to earlier Lateglacial advances. Boxleitner *et al.* (2019) dated 34
43
44 223 moraine boulders of several glacier systems in Meiental (central Alps), but we deliberately did
45
46 224 not consider the study in our test, because each moraine was dated with only one boulder.
47
48 225 Applying a realistic snow cover correction to all sites would equally shift all moraine ages to
49
50 226 slightly older dates and would not affect the discussion.
51
52
53
54
55
56
57
58
59
60

228 Results

229 *Geomorphological description of the Talèfre site*

230

231 Two massive lateral moraines, up to 50 m high and 1 km long, frame the islet of the “Jardin de
232 Talèfre” (purple moraines, including T4, in Fig. 2B and Fig. 3). In the eastern part of the islet,
233 three very smooth lateral moraine ridges (T1, T2 and T3) are visible in stratigraphically older
234 location relative to the massive moraine T4 on the eastern margin. They are less than 2 m high
235 and between 100 and 200 m long. The two outermost of these three moraine ridges (T1 and T2)
236 bear several large boulders suitable for ^{10}Be dating, while the ridge T3 does not. These three
237 ridges (T1 to T3) are represented in dark blue in Fig. 2B and Fig. 3. Moraine mapping shows
238 that they are leaning northward against a 20 m high rock slope at an altitude of ~ 2850 m a.s.l.;
239 to the south, they are crosscut by the T4 moraine. Between the western massive ridge and the
240 present glacier margin, a small ridge (T5) is visible (pink moraine in Fig. 3). It has no equivalent
241 on the eastern side and has been probably deposited during one of the short advances/stillstands
242 that occurred at Alpine sites during the general glacier retreat of the 20th century
243 (Schimmelpfennig *et al.* 2014; Braumann *et al.* 2020).

244

245 *Moraine and bedrock exposure ages of Talèfre glacier*

246

247 The two bedrock surfaces were sampled at the center of the northern part of the “Jardin de
248 Talèfre”. Moraine boulder samples were taken from three ridges in the eastern part of the islet,
249 i.e. from the two stratigraphically outermost (oldest), smooth moraines T1 and T2, and from
250 the innermost (youngest), massive moraine T4. Surface exposure ages are shown in Fig. 3 and
251 detailed in Table 1. Probability plots of moraine boulder ages and arithmetic mean ages are
252 shown in Fig. 4. The consistency of individual ages within one moraine age populations were

1
2
3 253 tested for outliers with the χ^2 test (2σ) by Ward & Wilson (1978), using the analytical
4
5 254 uncertainties of the ages. In the text and in figures, individual ages are given with the analytical
6
7
8 255 uncertainties, to allow for internal comparison, and arithmetic mean ages are given with their
9
10 256 standard deviations, while Table 1 shows both analytical uncertainties and total uncertainties
11
12 257 (including the ^{10}Be rate uncertainty). See figure and table captions for details.

13
14 258 All ages are in agreement with their stratigraphic order. The two bedrock samples, JDT-
15
16 259 16-1 and JDT-16-2, give indistinguishable exposure ages of 12.4 ± 0.4 and 12.3 ± 0.3 ka,
17
18 260 respectively. The three boulder ages from the outermost moraine T1 range between 12.2 ± 0.4
19
20 261 and 11.6 ± 0.3 ka, with a mean age of 12.0 ± 0.4 ka. Three boulder ages from moraine T2 are very
21
22 262 well clustered between 11.4 ± 0.3 and 11.1 ± 0.3 ka and give a mean age of 11.2 ± 0.2 ka after
23
24 263 discarding JDT-16-20 as an outlier (10.2 ± 0.3 ka). This boulder is less than 1 m high. It might
25
26 264 thus have been exhumed or covered for a while by a layer of sediment, leading to an
27
28 265 underestimation of its exposure age. On the innermost moraine, four boulders yield ages of
29
30 266 0.18 ± 0.02 , 0.22 ± 0.03 , 0.26 ± 0.02 and 0.33 ± 0.03 ka and one boulder is dated at 2.12 ± 0.07 ka.

31
32
33 267 According to this new set of exposure ages we propose a reconstruction of the past
34
35 268 extents of Talèfre glacier, corresponding to moraines T1 and T4 (Fig. 5). The mapping of the
36
37 269 exterior glacier margins relies solely on remnants of undated moraines, assumed variations in
38
39 270 relation to catchment slopes, and 19th century maps from French État-Major.

40
41
42 271

43 272 *Exposure ages of other Alpine chronologies*

44
45 273

46
47 274 The previously published 18 Alpine glacier chronologies that are considered here are
48
49 275 characterized by sets of lateral and/or latero-frontal moraines originally dated between ~ 13.5
50
51 276 and ~ 9.5 ka. Of these 18 sites, 11 meet the quality criteria presented in the section
52
53 277 “Methodology” and yield recalculated ^{10}Be exposure ages between 14.5 and 9.8 ka. The
54
55
56
57
58
59
60

1
2
3 278 moraine ages of the other sites are either older (Val Viola, Gesso della Barra valley, Romanche
4
5 279 valley, Great Aletsch glacier, Ferwall site) or show large standard deviations (Clarée valley).
6
7
8 280 Probability curves for all retained moraine mean ages in each site are plotted in Fig. 6 in
9
10 281 comparison with the Talèfre glacier moraine ages.

11
12 28213
14
15 283 Discussion16
17 284 *Oscillations of Talèfre glacier since the Younger Dryas*18
19 28520
21
22 286 According to the exposure ages of the two bedrock samples, the “Jardin de Talèfre” deglaciation
23
24 287 started at ~12.4 ka, i.e. during the YD period, if a continuous exposure scenario is assumed.25
26 288 Alternatively, the duration of ~12.4 ka could be composed of several exposure periods, e.g. a27
28 289 few hundred years of ice-free conditions during the warmer Bølling/Allerød (~14.7 – 12.9 ka;29
30 290 Lotter *et al.* 2000; Rasmussen *et al.* 2006) and subsequent burial by the re-advancing glacier at31
32 291 the beginning of the YD. However, the only slightly younger mean age of moraine T1 (12.0 ± 0.4 33
34 292 ka) implies that “Jardin de Talèfre” was deglaciated during the YD and the central rock islet35
36 293 has remained ice-free since that time. The mean ages of moraines T1 and T2 are37
38 294 stratigraphically consistent (12.0 ± 0.4 and 11.2 ± 0.2 ka) and coincide with the YD/EH transition.39
40 295 We propose that the T3 moraine was deposited during the EH, as its morphology is very similar41
42 296 to T1 and T2 moraines. This suggests that the glacier underwent at least three advances or43
44 297 stillstands after the beginning of its retreat ~12.4 ka ago until the EH.45
46 298 Four out of the five ages acquired from moraine T4 span from 0.18 ± 0.02 to 0.33 ± 0.03 47
48 299 ka, with a mean age of 0.25 ± 0.06 ka. These results indicate that the moraine was last overtopped49
50 300 at the end of the LIA, when several closely-spaced advances occurred. One out of the five51
52 301 samples of T4 is significantly older, 2.12 ± 0.07 ka (JDT-16-3). This older age can be either53
54 302 explained by isotope inheritance from a previous exposure duration or by accretion phases of

1
2
3 303 this massive moraine that pre-dated the deposition of the LIA boulders. Such advances prior to
4
5 304 the LIA have been reported for other glaciers in the French Alps: between ~3.5 and 0.7 ka at
6
7
8 305 Mer de Glace (Le Roy *et al.* 2015) and ~2.1 ka at Argentière glacier (Le Roy 2012) and in the
9
10 306 Ecrins-Pelvoux massif (Le Roy *et al.* 2017). However, our data do not allow us to decide which
11
12 307 of the two hypotheses is more likely.

13
14
15 308 Fig. 5 shows the large YD/EH and LIA extents of Talèfre glacier in comparison to that
16
17 309 of 2008. During the YD/EH and the LIA, the glacier is still connected with the Mer de Glace,
18
19 310 and the LIA extent is only slightly smaller than that of the YD/EH, while in 2008 the glacier
20
21 311 size is significantly reduced.

22
23
24 312 We do not have any evidence of glacier advances between the EH and the Late
25
26 313 Holocene, which is consistent with a warmer and dryer climate, and thus unfavorable for glacier
27
28 314 growth in the Alps, during this period (Ivy-Ochs *et al.* 2009). Therefore, we assume that Talèfre
29
30 315 glacier was smaller than its LIA extent during this period.

31
32
33 316

34 35 317 *Comparison with other Alpine glacier chronologies*

36
37
38 318

39
40 319 The YD/Holocene chronology of Talèfre glacier is very similar to the one recently established
41
42 320 at the nearby Argentière glacier (Protin *et al.* 2019). A similar set of bedrock surfaces (~2450
43
44 321 m a.s.l.) and five lateral moraines (~2400 - 2150 m a.s.l.), dated by *in situ* cosmogenic ¹⁰Be to
45
46 322 between ~11.7 and ~10.4 ka, provide evidence of deglaciation at the end of the YD and at least
47
48 323 five glacier re-advances or stillstands during the YD/EH transition. When comparing these two
49
50 324 age sets (Fig. 6D, E), it appears that the ages of the two outermost moraines of both glaciers are
51
52 325 undistinguishable within uncertainties, and that both glaciers oscillated several times during the
53
54 326 YD/EH transition. In this comparison, it must be kept in mind that T3 moraine of Talèfre glacier
55
56 327 could not be dated but seems to be only slightly younger than T1 and T2 moraines (see section
57
58
59
60

1
2
3 328 “Moraine and bedrock exposure ages of Talèfre glacier”) and might therefore be similar to the
4
5 329 innermost EH ridge of Argentièrre glacier dated to 10.4 ± 0.2 ka. These moraines of Talèfre and
6
7
8 330 Argentièrre glaciers thus probably represent quasi-synchronous, successive glacier stillstands
9
10 331 within the dynamic YD/EH retreat from their larger early-YD extents.

11
12 332 Moraines at multiple other locations across the Alps have previously been assigned to
13
14 333 the YD/EH transition based on ^{10}Be dating. Eleven of them were selected here, based on their
15
16 334 data quality (see section “Exposure ages of other Alpine chronologies”), together with our new
17
18 335 Talèfre chronology for this regional compilation. They are geographically distributed across
19
20 336 the European Alps (France, Switzerland, Italy and Austria), situated between longitudes $\sim 6.5^\circ\text{E}$
21
22 337 and 10°E and latitudes 45.5°N and 47°N (Fig. 6). All of these twelve moraine chronologies
23
24 338 indicate deposition of at least one moraine between ~ 12 and ~ 10 ka ago, i.e. during the YD/EH
25
26 339 transition (Fig. 6). Further, at most sites, there is evidence of deposition of multiple lateral
27
28 340 and/or latero-frontal moraines during this period. Successive moraines are located quite close
29
30 341 to each other and in proximity to the LIA moraines, suggesting only slightly smaller glacier
31
32 342 extents during the LIA than during the YD/EH compared to today’s reduced glacier sizes like
33
34 343 at Talèfre glacier (Fig. 5). The highest spatial spread is found at Arsine glacier displaying
35
36 344 YD/EH frontal moraines that are located about 1 km downstream of the LIA moraines
37
38 345 (Schimmelpfennig *et al.* 2019). At several other sites in the Alps, lateral YD/EH moraines exist
39
40 346 within <300 m-distance from lateral LIA moraines (Schimmelpfennig *et al.* 2012, 2014; Moran
41
42 347 *et al.* 2016a; Hofmann 2018).

43
44 348 Thus, based on the consistency of the ^{10}Be cosmogenic exposure ages, we show here
45
46 349 that millennial-scale synchronous glacier fluctuations occurred in the European Alps, and that
47
48 350 glaciers oscillated multiple times at centennial or sub-centennial scale superposed on a general
49
50 351 retreat trend during the 12-10 ka period. However, based on the available datasets it is not
51
52 352 possible to temporally correlate specific moraines between sites or to give evidence of a decadal
53
54
55
56
57
58
59
60

1
2
3 353 or centennial-scale synchronicity of glacier dynamics within the ~12-10 ka period, because of
4
5
6 354 (i) the analytical and geomorphic uncertainties related to the dating method; (ii) the probably
7
8 355 incomplete preservation of the moraine records or no deposition of the moraine; and (iii)
9
10 356 undated ridges within the investigated moraine sequences at several sites.

11
12 357 For the sites where ELA depressions between the YD/EH transition and the LIA have
13
14 358 been calculated using the Accumulation Area Ratio (AAR) method with a ratio of 0.67 (Table
15
16 359 S1), no significant correlations between moraine ages and ELA depressions are observed (Fig.
17
18 360 S1). In fact, the large range of ELA depressions supports the findings by Boxleitner *et al.* (2019)
19
20 361 that indicate ELA depressions should not be used to temporally correlate moraines from
21
22 362 different valleys, as previously proposed by Maisch (1981). This reflects the fact that ELA
23
24 363 variations of individual glaciers might be significantly influenced by local precipitation
25
26 364 amounts and local glacier morphology, as well as the limitations of the AAR method (e.g.
27
28 365 Reitner *et al.* 2016; Boxleitner *et al.* 2019).
29
30
31
32

33 366

34
35 367 *Link of the Alpine glacier oscillations with regional climate*
36
37

38 368
39
40 369 Analysis of the geographical characteristics of the 12 selected sites implies that their millennial
41
42 370 synchronicity is independent of their altitude range (at present between 1500 and 3400 m a.s.l.),
43
44 371 orientation (all directions) and size (0.3 to 14 km²) (Fig. S1). In the absence of common
45
46 372 topographic characteristics of the glaciers, the only process to explain the millennial-scale
47
48 373 synchronous fluctuations of independent ice mass fluctuations across the European Alps is a
49
50 374 regional climatic signal that prevailed over local factors. Therefore, we compare here the
51
52 375 moraine chronologies with regional - and high-latitude - independent climate proxy records in
53
54 376 an effort to elucidate the spatial reach of the climatic evolution underlying the quasi-
55
56 377 simultaneous glacier oscillations across the European Alps within their dynamic retreat.
57
58
59
60

1
2
3 378 Glaciers are sensitive to a variety of climatic factors, but the main driver for large-scale, long-
4
5 379 term glacier fluctuations in the mid- and high latitudes is the impact of summer temperature
6
7
8 380 variations (e.g. Oerlemans 2005; Solomina *et al.* 2015) on which we therefore focus. In
9
10 381 addition, over the last century, annual mass balance of Alpine glaciers was mainly driven by
11
12 382 summer melting (Huss *et al.* 2010). In the Alpine and pre-Alpine region, evidence of a
13
14 383 temperature minimum in the middle of the YD and several distinct cold events during a general
15
16
17 384 warming trend within the 12-10 ka period comes from various high-resolution palaeorecords
18
19 385 that reflect variations either in July air temperatures (based on chironomid-inferred records
20
21 386 from lakes in eastern France and the northern and central Swiss Alps; Heiri *et al.* 2015; Fig.
22
23 387 6A(3)) or in mean annual temperatures, based on stable isotope measurements in stalagmites
24
25 388 (Wurth *et al.* 2004; Affolter *et al.* 2019; Fig. 6A(2)) and biogenically precipitated carbonates in
26
27 389 lake sediments (Schwander *et al.* 2000). These decadal to centennial cold peaks seem to have
28
29 390 amplitudes in the order of ~ 0.5 °C, i.e. similar to the multidecadal fluctuations that drove the
30
31 391 succession of LIA moraines in the Alps (Oerlemans 2005). Regional cold peaks could therefore
32
33 392 be sufficient to lead to the YD/EH succession of glacial culminations or still-stands during the
34
35 393 general deglaciation observed in the Alps. In this case, it is most likely that decadal to centennial
36
37 394 glacier oscillations occurred quasi-simultaneously across the Alps.
38
39
40
41
42
43

44 396 *Link of the Alpine glacier extents with seasonality*

45
46 397
47
48 398 It is remarkable that several glaciers around 12 ka ago, i.e. at the end of the YD, were only
49
50 399 slightly larger than during the EH. This is the case for Rougnoux valley, Arsine, Talèfre,
51
52 400 Argentière, Tsidjiore Nouve, Belalp and Falgin Cirque glaciers, where the ages of the outermost
53
54 401 moraine fall into the YD or their uncertainties overlap with it (green probability curves in Fig.
55
56 402 6) and the ages of the innermost moraine fall into the EH. This small difference between late
57
58
59
60

1
2
3 403 YD and EH glacier extents seems inconsistent with the drastic YD temperature cooling and
4
5 404 abrupt mean annual temperature increase that characterizes the boundary between these two
6
7 405 periods (Fig. 6A). A linear relationship between oxygen isotope record and temperature would
8
9 406 suggest that the coldest YD temperatures of the Greenland sites were only slightly higher than
10
11 407 those of the Last Glacial Maximum (e.g. Rasmussen *et al.* 2008) when Alpine glaciers reached
12
13 408 until the Alpine foreland (Ivy-Ochs *et al.* 2008). Much larger glacier extents might therefore be
14
15 409 expected during and at the end of the ~1 ka lasting YD, especially compared to the EH and
16
17 410 LIA. In addition, the ^{10}Be bedrock ages from outboard of the oldest dated moraines of Talèfre
18
19 411 and Argentièrè glaciers suggest that these glaciers have been retreating prior to the deposition
20
21 412 of their respective late YD moraine. These results are in line with ^{10}Be -based glacier
22
23 413 chronologies from Greenland, also providing evidence of ice mass downwasting throughout the
24
25 414 YD, which lasted until the EH (Rainsley *et al.* 2018 and references therein).

26
27 415 The apparent mismatch between the glacier proxy records and the mean annual
28
29 416 temperature climate proxies could be due to a difference in seasonality between the YD and the
30
31 417 EH. This concept of seasonality was first proposed by Denton *et al.* (2005) to explain the
32
33 418 discord between the drastic change of the mean annual temperature observed in Greenland ice
34
35 419 cores and the slight snowline change of glaciers in Greenland and Europe during the YD and
36
37 420 EH. The YD, as well as other abrupt climate changes, has been qualified as a winter
38
39 421 phenomenon (Denton *et al.* 2005), meaning that the considerable annual temperature switches
40
41 422 observed in palaeoclimate records from Europe and Greenland are mainly due to changes in
42
43 423 winter temperature, while summer temperature did only undergo minor changes (Renssen &
44
45 424 Isarin 2001; Buizert *et al.* 2014; Schenk *et al.* 2018).

46
47 425 In the Alpine region, a decrease of the seasonality between the YD and EH is supported
48
49 426 by the difference of mean annual and summer warming estimated from the above-mentioned
50
51 427 recent independent proxy studies (Heiri *et al.* 2015; Affolter *et al.* 2019; Fig. 6A(2, 3)). The
52
53
54
55
56
57
58
59
60

1
2
3 428 stable isotope measurements in speleothems suggest an increase of the mean annual
4
5 429 temperature of ~ 5.4 °C at the YD/EH transition (Affolter *et al.* 2019; Fig. 6A(2)), while a
6
7
8 430 summer temperature increase of only ~ 2.7 °C is inferred from the chironomid-based lake
9
10 431 records (Heiri *et al.* 2015; Fig. 6A(3)). This difference between annual and summer temperature
11
12 432 could be explained by a greater winter warming of more than 7 °C if winter and summer periods
13
14 433 are assumed of equal duration. Furthermore, while the mean temperature increase in Greenland
15
16 434 occurred in less than one hundred years (Rasmussen *et al.* 2006; Fig. 6A(1)), the European
17
18 435 records indicate a more gradual warming distributed over several hundred years (Fig. 6A(2, 3)).
19
20 436 Our results support this concept, i.e. relatively mild YD summer temperatures could explain
21
22 437 why the glaciers in the Alps did not undergo a much more pronounced retreat at the YD/EH
23
24 438 transition, but glaciers retreated gradually from their only slightly larger YD extents.
25
26
27
28
29

439

440 *Link of the Alpine glacier oscillations with high latitude climate*

441

442 The clear correlation of high-resolution proxy records from the Alps and the Alpine foreland
443 (Heiri *et al.* 2015; Affolter *et al.* 2019; Fig. 6A(2, 3)) with the pattern of oxygen isotope
444 variations in Greenland ice cores (e.g. Rasmussen *et al.* 2006; Fig. 6A(1)) strongly suggests a
445 climatic link of the Alpine region with the northern high latitudes. In this context, a recent study
446 by Young *et al.* (2020) provides evidence of a succession of re-advances or stillstands of
447 mountain glaciers, the Laurentide Ice Sheet and Greenland Ice Sheet in the Baffin Bay region
448 at ~ 11.8 - 11.6 , ~ 10.4 and ~ 9.3 ka. The striking similarity of these moraine-based chronologies
449 from and near western Greenland with those from the European Alps provide further evidence
450 of a teleconnection between both regions at that time and that the observed glacier fluctuations
451 were due to a common climate evolution on extra-regional, maybe even hemispheric scale.

60

1
2
3 452 The question arises which large-scale climate mechanisms led to this teleconnection and
4
5 453 the contrasted seasonality imprinted in the above-discussed summer temperature and mean
6
7 454 annual temperature records. The abrupt onset of the YD cooling and the cold peaks of the Late
8
9 455 YD and EH in the high latitudes are thought to have been triggered by freshwater input from
10
11 456 the Laurentide Ice Sheet into the North Atlantic (Jennings *et al.* 2015) leading to a reduction of
12
13 457 the Atlantic Meridional Ocean Circulation (AMOC) (Renssen *et al.* 2015). The related
14
15 458 development of expanded wintertime sea ice in the North Atlantic shifted the westerlies south
16
17 459 leading to wind-transported cool temperatures to Europe (Brauer *et al.* 2008; Bakke *et al.* 2009),
18
19 460 and therefore to the Alps. During the second half of the YD, brief sea-ice breakups were led by
20
21 461 incursions of the Atlantic circulation and were associated with a northwards migration of the
22
23 462 polar front and westerly storm tracks (Bakke *et al.* 2009) until the system abruptly switched to
24
25 463 the interglacial state at the onset of the Holocene (Rasmussen *et al.* 2006). The signature of
26
27 464 these climatic mechanisms is markedly imprinted in the abrupt variations of the mean annual
28
29 465 temperature proxy records, but to a lesser degree in the glacier mass balance fluctuations.
30
31 466 Robust evidence of drastic glacier expansion in the Alps and the high latitudes in relation with
32
33 467 the strong annual cooling observed in the first part of the YD is rare so far. Early to mid-YD
34
35 468 moraines are preserved at a few sites in the Alps and at other sites in the North Atlantic region
36
37 469 (e.g. Belalp and Aletsch Glacier, Kelly *et al.* 2004; Schindelwig *et al.* 2012; Julier Pass, Ivy-
38
39 470 Ochs 2015; Alaska, Young *et al.* 2019; Norway, Wittmeier *et al.* 2020), but the corresponding
40
41 471 glacier extents were relatively modest compared to significant annual temperature decrease. In
42
43 472 addition, the deglaciation during the YD/EH transition was rather gradual and punctuated by
44
45 473 closely-spaced short-lived re-advances or stillstands. This could be explained by several
46
47 474 mechanisms. Sea ice expansion occurs predominantly in winter and might therefore not directly
48
49 475 result in a summer temperature decrease. In addition, the drastic YD cooling recorded by the
50
51 476 mean annual temperature proxies was enhanced by an increased strength of wind only during
52
53
54
55
56
57
58
59
60

1
2
3 477 autumn, winter and spring, which transported cold air from the ice-covered North Atlantic
4
5 478 region and led to cool and dry winters in Europe (Brauer *et al.* 2008). This phenomenon did not
6
7 479 occur during summer due to atmospheric blocking of the cold westerlies over Fennoscandia
8
9 480 leading to warm summers during the YD (Schenk *et al.* 2018). Therefore, and because snowfall
10
11 481 was reduced during the dry winters of the cold periods, greater glacier expansion did not occur
12
13 482 at many sites. Nevertheless, summers were very short, probably because winter sea ice
14
15 483 expansion lasted for a long period of the year, leading to a reduced glacier melt season (Young
16
17 484 *et al.* 2020). This might explain why glaciers responded with successive glacier advances or
18
19 485 stillstands to these dynamic changes in seasonality both in high latitudes and Europe.
20
21
22
23
24 486

25 26 487 Conclusions

27
28 488
29
30
31 489 Our new chronology based on 14^{10}Be cosmogenic exposure ages on moraine and bedrock from
32
33 490 the “Jardin de Talèfre” suggests that the central rock islet of the “Jardin de Talèfre” was
34
35 491 deglaciated during the YD and that Talèfre glacier retreated from its YD position starting ~ 12.4
36
37 492 ka ago. This retreat was interrupted by several episodes of stillstands before a major retreat
38
39 493 during the EH. No evidence of re-advances before the Late Holocene is recorded and the most
40
41 494 remarkable advance occurred during the LIA, which was only slightly less extensive than the
42
43 495 late YD and EH glacier extents at our high-elevation site. This behaviour is very similar to that
44
45 496 of the nearby Argentièrè glacier. The comparison of the YD/EH transition moraine chronology
46
47 497 of Talèfre glacier with those of 11 other Alpine glaciers scattered throughout the Alps suggests
48
49 498 a period of roughly synchronous glacial behaviour across the Alps between 12 and 10 ka ago.
50
51 499 Several glaciers deposited multiple moraines, which attest to regional-scale stillstands or re-
52
53 500 advances during the deglaciation. Similarities with palaeotemperature records from the Alpine
54
55 501 region as well as with glacial culminations and temperature records from Greenland strongly
56
57
58
59
60

1
2
3 502 suggest not only a regional common climate driver, but also a teleconnection with the high
4
5 503 latitudes, thus reinforcing the hypothesis postulated in earlier studies of a link between YD and
6
7 504 EH Alpine glacier fluctuations and Greenland climate change. However, the relatively small
8
9 505 amplitude of the YD glacier extents compared to the Holocene glacier extents is inconsistent
10
11 506 with the large and abrupt temperature shifts imprinted in mean annual proxy records in both
12
13 507 regions. We suggest that this inconsistency is due to a pronounced change in seasonality, with
14
15 508 YD winters cold and dry and YD summers only slightly cooler than those of the EH. This
16
17 509 seasonality difference controlled YD glacier extents and led to YD glaciers only slightly larger
18
19 510 than during the EH.
20
21
22
23
24
25

26 512 *Acknowledgements.* - This study is part of ANR 14-CE03-0006 VIP Mont-Blanc. We thank
27
28 513 Laëtitia Léanni (CEREGE) for support during chemistry and Jean Hanley and Roseanne
29
30 514 Schwartz (LDEO, Columbia University) for advices on sample chemistry and Joerg Schaefer
31
32 515 (LDEO, Columbia University) for discussion. The ASTER AMS national facility (CEREGE)
33
34 516 is supported by the INSU/CNRS, the ANR through the “projet thématiques d’excellence”
35
36 517 program for the “Equipements d’excellence” ASTER-CEREGE action and IRD. An earlier
37
38 518 version of this manuscript greatly benefitted from constructive comments by Benjamin
39
40 519 Chandler. We thank Marie Chenet and an anonymous reviewer whose relevant comments have
41
42 520 helped to improve this manuscript.
43
44
45
46
47
48

49 522 *Author contributions.* - JLM, IS, JFB and BP acquired the funding for the project leading to this
50
51 523 publication. MP, JLM, JFB, BP and LM conducted the fieldwork. MP carried out the laboratory
52
53 524 work. ASTER Team realized the AMS measurements. MP, IS, JLM and MLR did the data
54
55 525 analysis and prepared the original draft of the manuscript and all co-authors contributed the
56
57 526 final draft of the manuscript.
58
59
60

1
2
3 527
4
5 528 *Data availability.* - The data that support the findings of this study are available from the
6
7
8 529 corresponding author upon reasonable request.
9

10 530

11
12 531 **References**

13
14
15 532 Affolter, S., Häuselmann, A., Fleitmann, D., Edwards, R. L., Cheng, H. & Leuenberger, M.

16
17 533 2019: Central Europe temperature constrained by speleothem fluid inclusion water

18
19 534 isotopes over the past 14,000 years. *Science Advances* 5, eaav3809,

20
21 535 <https://doi.org/10.1126/sciadv.aav3809>.
22
23

24 536 André, M. 2002: Rates of postglacial rock weathering on glacially scoured outcrops (abisko–

25
26 537 riksgården area, 68°N). *Geografiska Annaler: Series A, Physical Geography* 84, 139–

27
28 538 150.
29
30

31 539 Arnold, M., Merchel, S., Bourlès, D. L., Braucher, R., Benedetti, L., Finkel, R.C., Aumaître,

32
33 540 G., Gottdang, A. & Klein, M. 2010: The French accelerator mass spectrometry facility

34
35 541 ASTER: Improved performance and developments. *Nuclear Instruments and Methods in*

36
37 542 *Physics Research Section B: Beam Interactions with Materials and Atoms* 268, 1954–

38
39 543 1959.
40
41

42 544 Bakke, J., Lie, Ø., Heegaard, E., Dokken, T., Haug, G. H., Birks, H. H., Dulski, P. & Nilsen,

43
44 545 T. 2009: Rapid oceanic and atmospheric changes during the Younger Dryas cold period.

45
46 546 *Nature Geoscience* 2, 202–205.
47
48

49 547 Balco, G., Stone, J. O., Lifton, N. A. & Dunai, T. J. 2008: A complete and easily accessible

50
51 548 means of calculating surface exposure ages or erosion rates from ^{10}Be and ^{26}Al

52
53 549 measurements. *Quaternary Geochronology* 3, 174–195.
54
55

56 550 Balco, G., Briner, J., Finkel, R. C., Rayburn, J. A., Ridge, J. C. & Schaefer, J. M. 2009: Regional

57
58 551 beryllium-10 production rate calibration for late-glacial northeastern North America.
59
60

- 1
2
3 552 *Quaternary Geochronology* 4, 93–107.
4
5 553 Balco, G. 2017: Production rate calculations for cosmic-ray-muon-produced ^{10}Be and ^{26}Al
6
7 554 benchmarked against geological calibration data. *Quaternary Geochronology* 39, 150-
8
9 555 173.
10
11 556 Baroni, C., Casale, S., Salvatore, M. C., Ivy-Ochs, S., Christl, M., Carturan, L., Seppi, R. &
12
13 557 Carton, A. 2017: Double response of glaciers in the Upper Peio Valley (Rhaetian Alps,
14
15 558 Italy) to the Younger Dryas climatic deterioration. *Boreas* 46, 783–798.
16
17 559 Borchers, B., Marrero, S., Balco, G., Caffee, M., Goehring, B., Lifton, N., Nishiizumi, K.,
18
19 560 Phillips, F., Schaefer, J. & Stone, J. 2016: Geological calibration of spallation production
20
21 561 rates in the CRONUS-Earth project. *Quaternary Geochronology* 31, 188–198.
22
23 562 Boxleitner, M., Ivy-Ochs, S., Egli, M., Brandova, D., Christl, M. & Maisch, M. 2019:
24
25 563 Lateglacial and Early Holocene glacier stages - New dating evidence from the Meiental
26
27 564 in central Switzerland. *Geomorphology* 340, 15-31.
28
29 565 Braucher, R., Guillou, V., Bourlès, D. L., Arnold, M., Aumaître, G., Keddadouche, K. &
30
31 566 Nottoli, E. 2015: Preparation of ASTER in-house $^{10}\text{Be}/^9\text{Be}$ standard solutions. *Nuclear*
32
33 567 *Instruments and Methods in Physics Research Section B: Beam Interactions with*
34
35 568 *Materials and Atoms* 361, 335–340.
36
37 569 Brauer, A., Haug, G. H., Dulski, P., Sigman, D. M. & Negendank, J. F. W. 2008: An abrupt
38
39 570 wind shift in western Europe at the onset of the Younger Dryas cold period. *Nature*
40
41 571 *Geoscience* 1, 520–523.
42
43 572 Braumann, S. M., Schaefer, J. M., Neuhuber, S. M., Reitner, J. M., Lüthgens, C. & Fiebig, M.
44
45 573 2020: Holocene glacier change in the Silvretta Massif (Austrian Alps) constrained by a
46
47 574 new ^{10}Be chronology, historical records and modern observations. *Quaternary Science*
48
49 575 *Reviews* 245, 106493, <https://doi.org/10.1016/j.quascirev.2020.106493>.
50
51 576 Buizert, C., Gkinis, V., Severinghaus, J. P., He, F., Lecavalier, B. S., Kindler, P., Leuenberger,
52
53
54
55
56
57
58
59
60

- 1
2
3 577 M., Carlson, A. E., Vinther, B., Masson-Delmotte, V., White, J. W. C., Liu, Z., Otto-
4
5 578 Bliesner, B. & Brook, E. J. 2014: Greenland temperature response to climate forcing
6
7 579 during the last deglaciation. *Science* 345, 1177–1180.
8
9
10 580 Bussy, F., Hernandez, J. & Raumer, J. V. 2000. Bimodal magmatism as a consequence of the
11
12 581 post-collisional readjustment of the thickened Variscan continental lithosphere (Aiguilles
13
14 582 Rouges-Mont Blanc Massifs, Western Alps). *Earth and Environmental Science*
15
16 583 *Transactions of the Royal Society of Edinburgh* 91, 221–233.
17
18
19 584 Chenet, M., Brunstein, D., Jomelli, V., Roussel, E., Rinterknecht, V., Mokadem, F., Biette, M.,
20
21 585 Robert, V. & Léanni, L. 2016: ^{10}Be cosmic-ray exposure dating of moraines and rock
22
23 586 avalanches in the Upper Romanche valley (French Alps): Evidence of two glacial
24
25 587 advances during the Late Glacial/Holocene transition. *Quaternary Science Reviews* 148,
26
27 588 209–221.
28
29
30 589 Chmeleff, J., von Blanckenburg, F., Kossert, K. & Jakob, D. 2010: Determination of the ^{10}Be
31
32 590 half-life by multicollector ICP-MS and liquid scintillation counting. *Nuclear Instruments*
33
34 591 *and Methods in Physics Research Section B: Beam Interactions with Materials and Atoms*
35
36 592 268, 192–199.
37
38
39 593 Claude, A., Ivy-Ochs, S., Kober, F., Antognini, M., Salcher, B. & Kubik, P. W. 2014: The
40
41 594 Chironico landslide (Valle Leventina, southern Swiss Alps): age and evolution. *Swiss*
42
43 595 *Journal of Geosciences* 107, 273–291.
44
45
46 596 Cossart, E., Fort, M., Boursières, D., Braucher, R., Perrier, R. & Siame, L. 2012: Deglaciation
47
48 597 pattern during the Lateglacial/Holocene transition in the southern French Alps.
49
50 598 Chronological data and geographical reconstruction from the Clarée Valley (upper
51
52 599 Durance catchment, southeastern France). *Palaeogeography, Palaeoclimatology,*
53
54 600 *Palaeoecology* 315–316, 109–123.
55
56
57 601 de Decker Heftler, S. 2002: Photographier le Mont Blanc. 171 pp. Editions Guérin, Chamonix.
58
59
60

- 1
2
3 602 Denton, G., Alley, R., Comer, G. & Broecker, W. 2005: The role of seasonality in abrupt
4
5 603 climate change. *Quaternary Science Reviews* 24, 1159–1182.
6
7
8 604 Fischer, M., Huss, M., Barboux, C. & Hoelzle, M. 2014: The New Swiss Glacier Inventory
9
10 605 SGI2010: Relevance of Using High-Resolution Source Data in Areas Dominated by Very
11
12 606 Small Glaciers. *Arctic, Antarctic, and Alpine Research* 46, 933–945.
13
14
15 607 Gardent, M. 2014: *Inventaire et retrait des glaciers dans les alpes françaises depuis la fin du*
16
17 608 *Petit Age Glaciaire*. Ph.D. thesis, Université de Grenoble, 444 pp.
18
19 609 Gardent, M., Rabatel, A., Dedieu, J.-P. & Deline, P. 2014: Multitemporal glacier inventory of
20
21 610 the French Alps from the late 1960s to the late 2000s. *Global and Planetary Change* 120,
22
23 611 24–37.
24
25
26 612 Heiri, O., Ilyashuk, B., Millet, L., Samartin, S. & Lotter, A. F. 2015: Stacking of discontinuous
27
28 613 regional palaeoclimate records: Chironomid-based summer temperatures from the Alpine
29
30 614 region. *The Holocene* 25, 137–149.
31
32
33 615 Hofmann, F. M. 2018: Glacial history of the upper Drac Blanc catchment (Écrins massif,
34
35 616 French Alps). *E&G Quaternary Science Journal* 67, 37–40.
36
37
38 617 Huss, M., Hock, R., Bauder, A. & Funk, M. 2010: 100-year mass changes in the Swiss Alps
39
40 618 linked to the Atlantic Multidecadal Oscillation. *Geophysical Research Letters* 37,
41
42 619 <https://doi.org/10.1029/2010GL042616>.
43
44
45 620 Ivy-Ochs, S. 2015: Glacier variations in the European Alps at the end of the last glaciation.
46
47 621 *Cuadernos de Investigación Geográfica* 41, 295-315.
48
49 622 Ivy-Ochs, S., Kerschner, H., Reuther, A., Maisch, M., Sailer, R., Schaefer, J., Kubik, P. W.,
50
51 623 Synal, H.-A. & Schlüechter, C. 2006: The timing of glacier advances in the northern
52
53 624 European Alps based on surface exposure dating with cosmogenic ^{10}Be , ^{26}Al , ^{36}Cl , and
54
55 625 ^{21}Ne . In Alonso-Zarza, A. M. & Tanner, L. H. (eds.): *In Situ-Produced Cosmogenic*
56
57 626 *Nuclides and Quantification of Geological Processes*, 43– 60. Geological Society of
58
59
60

1
2
3 627 America, Boulder.
4

5 628 Ivy-Ochs, S., Kerschner, H., Reuther, A., Preusser, F., Heine, K., Maisch, M., Kubik, P. W. &
6

7 629 Schlüchter, C. 2008: Chronology of the last glacial cycle in the European Alps. *Journal*
8

9
10 630 *of Quaternary Science* 23, 559–573.
11

12 631 Ivy-Ochs, S., Kerschner, H., Maisch, M., Christl, M., Kubik, P. W. & Schlüchter, C. 2009:
13

14 632 Latest Pleistocene and Holocene glacier variations in the European Alps. *Quaternary*
15

16 633 *Science Reviews* 28, 2137–2149.
17

18 634 Jennings, A., Andrews, J., Pearce, C., Wilson, L. & Ólfasdóttir, S. 2015: Detrital carbonate
19

20 635 peaks on the Labrador shelf, a 13–7ka template for freshwater forcing from the Hudson
21

22 636 Strait outlet of the Laurentide Ice Sheet into the subpolar gyre. *Quaternary Science*
23

24 637 *Reviews* 107, 62–80.
25

26 638 Joly, D., Berger, A., Buoncristiani, J.-F., Champagne, O., Pergaud, J., Richard, Y., Soare, P. &
27

28 639 Pohl, B. 2018: Geomatic downscaling of temperatures in the Mont Blanc massif: A NEW
29

30 640 STATISTICAL DOWNSCALING APPROACH. *International Journal of Climatology*
31

32 641 38, 1846–1863.
33

34 642 Jordan, D. 2010: Le Jardin de Talèfre dans le massif du Mont-Blanc à Chamonix - Réévaluation
35

36 643 et contribution à sa connaissance botanique. *Le Monde des Plantes* 501, 9-20.
37

38 644 Kelly, M. A., Kubik, P. W., Von Blanckenburg, F. & Schlüchter, C. 2004: Surface exposure
39

40 645 dating of the Great Aletsch Glacier Egesen moraine system, western Swiss Alps, using
41

42 646 the cosmogenic nuclide ^{10}Be . *Journal of Quaternary Science* 19, 431–441.
43

44 647 Kerschner, H., Hertl, A., Gross, G., Ivy-Ochs, S. & Kubik, P. W. 2006: Surface exposure dating
45

46 648 of moraines in the Kromer valley (Silvretta Mountains, Austria)-evidence for glacial
47

48 649 response to the 8.2 ka event in the Eastern Alps? *The Holocene* 16, 7–15.
49

50 650 Kobashi, T., Severinghaus, J. P. & Barnola, J.-M. 2008: 4 ± 1.5 °C abrupt warming 11,270 yr
51

52 651 ago identified from trapped air in Greenland ice. *Earth and Planetary Science Letters*
53
54
55
56
57
58
59
60

- 1
2
3 652 268, 397–407.
4
5 653 Korschinek, G., Bergmaier, A., Faestermann, T., Gerstmann, U. C., Knie, K., Rugel, G.,
6
7 654 Wallner, A., Dillmann, I., Dollinger, G., von Gostomski, Ch. L., Kossert, K., Maiti, M.,
8
9 655 Poutivtsev, M. & Remmert, A. 2010: A new value for the half-life of ^{10}Be by Heavy-Ion
10
11 656 Elastic Recoil Detection and liquid scintillation counting. *Nuclear Instruments and*
12
13 657 *Methods in Physics Research Section B: Beam Interactions with Materials and Atoms*
14
15 658 268, 187–191.
16
17 659 Le Roy, M. 2012: *Reconstitution des fluctuations glaciaires Holocènes dans les Alpes*
18
19 660 *occidentales: apports de la dendrochronologie et de la datation par isotopes*
20
21 661 *cosmogéniques produits in situ*. Ph.D. thesis, Université Grenoble Alpes, 363 pp.
22
23 662 Le Roy, M., Nicolussi, K., Deline, P., Astrade, L., Edouard, J.-L., Miramont, C. & Arnaud, F.
24
25 663 2015: Calendar-dated glacier variations in the western European Alps during the
26
27 664 Neoglacial: the Mer de Glace record, Mont Blanc massif. *Quaternary Science Reviews*
28
29 665 108, 1–22.
30
31 666 Le Roy, M., Deline, P., Carcaillet, J., Schimmelpfennig, I. & Ermini, M. 2017: ^{10}Be exposure
32
33 667 dating of the timing of Neoglacial glacier advances in the Ecrins-Pelvoux massif,
34
35 668 southern French Alps. *Quaternary Science Reviews* 178, 118–138.
36
37 669 Lotter, A. F., Birks, H. J. B., Eicher, U., Hofmann, W., Schwander, J. & Wick, L. 2000:
38
39 670 Younger Dryas and Allerød summer temperatures at Gerzensee (Switzerland) inferred
40
41 671 from fossil pollen and cladoceran assemblages. *Palaeogeography, Palaeoclimatology,*
42
43 672 *Palaeoecology* 159, 349–361.
44
45 673 Maisch, M. 1981: *Glazialmorphologische und gletschergeschichtliche Untersuchungen im*
46
47 674 *Gebiet zwischen Landwasser- und Albulatal (Kt. Graubünden, Schweiz)*. Ph.D. thesis,
48
49 675 Universität Zürich, 215 pp.
50
51 676 Marsicek, J., Shuman, B. N., Bartlein, P. J., Shafer, S. L. & Brewer, S. 2018: Reconciling
52
53
54
55
56
57
58
59
60

- 1
2
3 677 divergent trends and millennial variations in Holocene temperatures. *Nature* 554, 92–96.
4
5 678 Martin, L. C. P., Blard, P.-H., Balco, G., Lavé, J., Delunel, R., Lifton, N. & Laurent, V. 2017:
6
7 679 The CREp program and the ICE-D production rate calibration database: A fully
8
9 680 parameterizable and updated online tool to compute cosmic-ray exposure ages.
10
11 681 *Quaternary Geochronology* 38, 25–49.
12
13
14 682 Merchel, S., Arnold, M., Aumaître, G., Benedetti, L., Bourlès, D. L., Braucher, R., Alfimov,
15
16 683 V., Freeman, S. P. H. T., Steier, P. & Wallner, A. 2008: Towards more precise ^{10}Be and
17
18 684 ^{36}Cl data from measurements at the 10–14 level: Influence of sample preparation. *Nuclear*
19
20 685 *Instruments and Methods in Physics Research Section B: Beam Interactions with*
21
22 686 *Materials and Atoms* 266, 4921–4926.
23
24
25 687 Moran, A. P., Ivy-Ochs, S., Schuh, M., Christl, M. & Kerschner, H. 2016a: Evidence of central
26
27 688 Alpine glacier advances during the Younger Dryas–early Holocene transition period.
28
29 689 *Boreas* 45, 398–410.
30
31
32 690 Moran, A. P., Kerschner, H. & Ochs, S. I. 2016b: Redating the moraines in the Kromer Valley
33
34 691 (Silvretta Mountains)—New evidence for an early Holocene glacier advance. *The*
35
36 692 *Holocene* 26, 655–664.
37
38
39 693 Oerlemans, J. 2005: Extracting a climate signal from 169 glacier records. *Science* 308, 675–
40
41 694 677.
42
43
44 695 Protin, M., Schimmelpfennig, I., Mugnier, J.-L., Ravanel, L., Le Roy, M., Deline, P., Favier,
45
46 696 V., Buoncristiani, J.-F. & ASTER Team 2019: Climatic reconstruction for the Younger
47
48 697 Dryas/Early Holocene transition and the Little Ice Age based on paleo-extents of
49
50 698 Argentièrè glacier (French Alps). *Quaternary Science Reviews* 221, 105863,
51
52 699 <https://doi.org/10.1016/j.quascirev.2019.105863>.
53
54
55 700 Prud'homme, C., Vassallo, R., Crouzet, C., Carcaillet, J., Mugnier, J.-L. & Cortés-Aranda, J.
56
57 701 2020: Paired ^{10}Be sampling of polished bedrock and erratic boulders to improve dating
58
59
60

- 1
2
3 702 of glacial landforms: an example from the Western Alps. *Earth Surface Processes and*
4
5 703 *Landforms* 45, 1168–1180.
- 6
7
8 704 Putnam, A. E., Bromley, G. R. M., Rademaker, K. & Schaefer, J. M. 2019: In situ ^{10}Be
9
10 705 production-rate calibration from a ^{14}C -dated late-glacial moraine belt in Rannoch Moor,
11
12 706 central Scottish Highlands. *Quaternary Geochronology* 50, 109–125.
- 13
14 707 Rabatel, A., Letréguilly, A., Dedieu, J.-P. & Eckert, N. 2013: Changes in glacier equilibrium-
15
16 708 line altitude in the western Alps from 1984 to 2010: evaluation by remote sensing and
17
18 709 modeling of the morpho-topographic and climate controls. *The Cryosphere* 7, 1455–
19
20 710 1471.
- 21
22
23 711 Rainsley, E., Menviel, L., Fogwill, C. J., Turney, C. S. M., Hughes, A. L. C. & Rood, D. H.
24
25 712 2018: Greenland ice mass loss during the Younger Dryas driven by Atlantic Meridional
26
27 713 Overturning Circulation feedbacks. *Scientific Reports* 8, 11307,
28
29 714 <https://doi.org/10.1038/s41598-018-29226-8>.
- 30
31
32 715 Rasmussen, S. O., Andersen, K. K., Svensson, A. M., Steffensen, J. P., Vinther, B. M., Clausen,
33
34 716 H. B., Siggaard-Andersen, M. L., Johnsen, S. J., Larsen, L. B., Dahl-Jensen, D., Bigler,
35
36 717 M., Rothlisberger, R., Fischer, H., Goto-Azuma, K., Hansson, M. E. & Ruth, U. 2006: A
37
38 718 new Greenland ice core chronology for the last glacial termination. *Journal of*
39
40 719 *Geophysical Research - Atmospheres* 111, D06102,
41
42 720 <https://doi.org/10.1029/2005JD006079>.
- 43
44
45 721 Rasmussen, S. O., Seierstad, I. K., Andersen, K. K., Bigler, M., Dahl-Jensen, D., Johnsen & S.
46
47 722 J. 2008: Synchronization of the NGRIP, GRIP, and GISP2 ice cores across MIS 2 and
48
49 723 palaeoclimatic implications. *Quaternary Science Reviews* 27, 18–28.
- 50
51
52 724 Reitner, J. M., Ivy Ochs, S., Dreschner-Schneider, R., Hajdas, I. & Linner, M. 2016:
53
54 725 Reconsidering the current stratigraphy of the Alpine Lateglacial: Implications of the
55
56 726 sedimentary and morphological record of the Lienz area (Tyrol/Austria). *E&G*
57
58
59
60

- 1
2
3 727 *Quaternary Science Journal* 65, 113-144.
4
5 728 Renssen, H. & Isarin, R. F. B. 2001: The two major warming phases of the last deglaciation at
6
7 729 ~14.7 and ~11.5 ka cal BP in Europe: climate reconstructions and AGCM experiments.
8
9 730 *Global and Planetary Change* 30, 117–153.
10
11
12 731 Renssen, H., Mairesse, A., Goosse, H., Mathiot, P., Heiri, O., Roche, D. M., Nisancioglu, K.
13
14 732 H. & Valdes, P. J. 2015: Multiple causes of the Younger Dryas cold period. *Nature*
15
16 733 *Geoscience* 8, 946–949.
17
18 734 Roe, G. H., Baker, M. B. & Herla, F. 2017: Centennial glacier retreat as categorical evidence
19
20 735 of regional climate change. *Nature Geoscience* 10, 95–99.
21
22
23 736 Schenk, F., Väliranta, M., Muschitiello, F., Tarasov, L., Heikkilä, M., Björck, S., Brandefelt,
24
25 737 J., Johansson, A. V., Näslund, J.-O. & Wohlfarth, B. 2018: Warm summers during the
26
27 738 Younger Dryas cold reversal. *Nature Communications* 9, 1634,
28
29 739 <https://doi.org/10.1038/s41467-018-04071-5>.
30
31
32 740 Schimmelpfennig, I., Schaefer, J. M., Goehring, B. M., Lifton, N., Putnam, A. E. & Barrell, D.
33
34 741 J. A. 2012: Calibration of the in situ cosmogenic ¹⁴C production rate in New Zealand's
35
36 742 Southern Alps. *Journal of Quaternary Science* 27, 671–674.
37
38
39 743 Schimmelpfennig, I., Schaefer, J. M., Akçar, N., Koffman, T., Ivy-Ochs, S., Schwartz, R.,
40
41 744 Finkel, R. C., Zimmerman, S. & Schlüchter, C. 2014: A chronology of Holocene and
42
43 745 Little Ice Age glacier culminations of the Steingletscher, Central Alps, Switzerland, based
44
45 746 on high-sensitivity beryllium-10 moraine dating. *Earth and Planetary Science Letters*
46
47 747 393, 220–230.
48
49
50 748 Schimmelpfennig, I., Le Roy, M., Deline, P., Schoeneich, P., Carcaillet, J., Bodin, X. & ASTER
51
52 749 Team 2019: Holocene dynamics of Arsine glacier (Ecrins massif, French Alps) inferred
53
54 750 from ¹⁰Be dating. Abstract, INQUA conference, Dublin.
55
56 751 <https://doi.org/10.13140/RG.2.2.10849.86884>.
57
58
59
60

- 1
2
3 752 Schindelwig, I., Akçar, N., Kubik, P. W. & Schlüchter, C. 2012: Lateglacial and early Holocene
4
5 753 dynamics of adjacent valley glaciers in the Western Swiss Alps. *Journal of Quaternary*
6
7 754 *Science* 27, 114–124.
- 8
9
10 755 Schwander, J., Eicher, U. & Ammann, B. 2000: Oxygen isotopes of lake marl at Gerzensee and
11
12 756 Leysin (Switzerland), covering the Younger Dryas and two minor oscillations, and their
13
14 757 correlation to the GRIP ice core. *Palaeogeography, Palaeoclimatology, Palaeoecology*
15
16 758 *159*, 203–214.
- 17
18
19 759 Shakun, J. D., Clark, P. U., He, F., Lifton, N.A., Liu, Z. & Otto-Bliesner, B. L. 2015: Regional
20
21 760 and global forcing of glacier retreat during the last deglaciation. *Nature*
22
23 761 *Communications* 6, 8059, <https://doi.org/10.1038/ncomms9059>.
- 24
25
26 762 Smiraglia, C., Azzoni, R. S., D'Agata, C., Maragno, D., Fugazza, D. & Diolaiuti, G. A. 2015:
27
28 763 The evolution of the Italian glaciers from the previous data base to the New Italian
29
30 764 Inventory. Preliminary considerations and results. *Geografia Fisica e Dinamica*
31
32 765 *Quaternaria* 38, 79–87.
- 33
34
35 766 Solomina, O. N., Bradley, R. S., Hodgson, D. A., Ivy-Ochs, S., Jomelli, V., Mackintosh, A. N.,
36
37 767 Nesje, A., Owen, L. A., Wanner, H., Wiles, G. C. & Young, N. E. 2015: Holocene glacier
38
39 768 fluctuations. *Quaternary Science Reviews* 111, 9–34.
- 40
41
42 769 Vincent, C., Fischer, A., Mayer, C., Bauder, A., Galos, S. P., Funk, M., Thibert, E., Six, D.,
43
44 770 Braun, L. & Huss, M. 2017: Common climatic signal from glaciers in the European Alps
45
46 771 over the last 50 years. *Geophysical Research Letters* 44, 1376–1383.
- 47
48
49 772 Vinther, B. M., Clausen, H. B., Johnsen, S. J., Rasmussen, S. O., Andersen, K. K., Buchardt,
50
51 773 S. L., Dahl-Jensen, D., Seierstad, I. K., Siggaard-Andersen, M.-L., Steffensen, J. P.,
52
53 774 Svensson, A., Olsen, J. & Heinemeier, J. 2006: A synchronized dating of three Greenland
54
55 775 ice cores throughout the Holocene. *Journal of Geophysical Research - Atmospheres* 111,
56
57 776 D13102, <https://doi.org/10.1029/2005JD006921>.
- 58
59
60

- 1
2
3 777 Ward, G. K. & Wilson, S. R. 1978: Procedures for comparing and combining radiocarbon age
4
5 778 determinations: a critique. *Archaeometry* 20, 19–31.
6
7
8 779 Wittmeier, H. E., Schaefer, J. M., Bakke, J., Rupper, S., Paasche, Ø., Schwartz, R. & Finkel,
9
10 780 R. C. 2020: Late Glacial mountain glacier culmination in Arctic Norway prior to the
11
12 781 Younger Dryas. *Quaternary Science Reviews* 245, 106461, doi:
13
14 782 10.1016/j.quascirev.2020.106461.
15
16
17 783 Wurth, G., Niggemann, S., Richter, D. K. & Mangini, A. 2004: The Younger Dryas and
18
19 784 Holocene climate record of a stalagmite from Hölloch Cave (Bavarian Alps, Germany).
20
21 785 *Journal of Quaternary Science* 19, 291–298.
22
23
24 786 Young, N. E., Schaefer, J. M., Briner, J. P. & Goehring, B. M. 2013. A ^{10}Be production-rate
25
26 787 calibration for the Arctic. *Journal of Quaternary Science* 28, 515–526.
27
28
29 788 Young, N. E., Briner, J. P., Schaefer, J., Zimmerman, S. & Finkel, R. C. 2019: Early Younger
30
31 789 Dryas glacier culmination in southern Alaska: Implications for North Atlantic climate
32
33 790 change during the last deglaciation. *Geology* 47, 550–554.
34
35
36 791 Young, N. E., Briner, J. P., Miller, G. H., Lesnek, A. J., Crump, S. E., Thomas, E. K., Pendleton,
37
38 792 S. L., Cuzzone, J., Lamp, J., Zimmerman, S., Caffee, M. & Schaefer, J. M. 2020:
39
40 793 Deglaciation of the Greenland and Laurentide ice sheets interrupted by glacier advance
41
42 794 during abrupt coolings. *Quaternary Science Reviews* 229, 106091,
43
44 795 <https://doi.org/10.1016/j.quascirev.2019.106091>.
45
46
47
48
49
50
51
52
53
54
55
56
57
58
59
60

1
2
3 796 Legends
4
5

6 797 Fig. 1. Location of Talèfre glacier and study area: the “Jardin de Talèfre”. A. Location of the
7
8 798 Mont Blanc massif (red dot) in the Alps (red dotted line). B. The Mont Blanc massif and
9
10 799 present-day glacier extents on a Landsat 8 image (April 2015); French glaciers: Gardent *et al.*
11
12 800 (2014); Swiss glaciers: Fischer *et al.* (2014); Italian glaciers: Smiraglia *et al.* (2015). Talèfre
13
14 801 glacier is highlighted in dark blue, the “Jardin de Talèfre” is located in the red square.
15
16
17
18 802

19
20 803 Fig. 2. A. Photograph of the “Jardin de Talèfre” in 1890 (source: "Les Amis du Vieux
21
22 804 Chamonix"). B. Oblique aerial imagery of the “Jardin de Talèfre” in September 2016. Talèfre
23
24 805 glacier is highlighted in light blue, sampled moraines T1 and T2 (dark blue) and Holocene
25
26 806 moraines, including T4 (purple) are shown. Bedrock sample locations are shown as red dots
27
28 807 and some of the sampled boulders as green dots (photograph by J.-F. Buoncristiani). C.
29
30 808 Example of sampled bedrock surface. D. Example of sampled boulder on T2 moraine.
31
32
33
34 809

35
36
37 810 Fig. 3. Moraines and sample locations in the “Jardin de Talèfre”, mapped on the 5 m IGN DEM
38
39 811 RGE ALTI and aerial images. Present-day glacier extent (in blue) is from Gardent *et al.* (2014).
40
41 812 Dashed lines represent undated moraines, the age of which is assumed according to their
42
43 813 relative position and morphology. Individual surface exposure ages are listed in the white boxes
44
45 814 with their analytical uncertainties and mean ages of the landforms in the colored bands
46
47 815 (arithmetic means and standard deviations). Outliers are in italic grey font.
48
49
50
51 816

52
53
54 817 Fig. 4. Probability plots of the individual moraine sample ages (black curves, analytical
55
56 818 uncertainty only) from Talèfre glacier. Colored curves, vertical lines and bands represent the
57
58
59
60

1
2
3 819 summed probability plots, arithmetic means and standard deviations, respectively,
4
5 820 corresponding to the age labeled in each box, only calculated for T1 and T2.
6

7 821
8
9
10 822 Fig. 5. Reconstruction of past extents of Talèfre glacier, based on mapping of the preserved
11
12 823 moraines and interpretation of ^{10}Be dating, for the Younger Dryas/Early Holocene transition
13
14 824 (A) (12 ka, stage T1 moraine), LIA maximum (B) and 2008 CE (C) (Gardent *et al.* 2014).
15
16 825 Dashed glacier limits correspond to hypothetical extents.
17
18
19

20 826
21
22 827 Fig. 6. Chronology of culminations of Talèfre glacier based on the ^{10}Be mean ages of the glacial
23
24 828 landforms in this study (D) compared to independent palaeoclimate records (A) and to other
25
26 829 glacier chronology studies in the Alps also using ^{10}Be moraine dating (B-M). Each moraine is
27
28 830 represented by a summed probability curve along with the number of dated boulders ($n = x$),
29
30 831 vertical lines and colored band represent the arithmetic means and standard deviations (1σ),
31
32 832 colors represent the stratigraphic order of the moraines (from outer to inner: green, blue, purple,
33
34 833 pink). A(1). Oxygen isotope record in Greenland ice core NGRIP (Rasmussen *et al.* 2006;
35
36 834 Vinther *et al.* 2006), blue bands represent the Younger Dryas and cold peaks during the Early
37
38 835 Holocene as identified in the Greenland ice core record. A(2). Oxygen isotope record from
39
40 836 speleotem fluid inclusion from Milandre cave, Switzerland (Affolter *et al.* 2019). A(3). Stacked
41
42 837 chironomid-inferred July air temperature from the Alps (Heiri *et al.* 2015), black arrows point
43
44 838 to peaks mentioned in the main text. Alpine glacier sites in panels B, C and E to M are presented
45
46 839 from east to west with their locations shown by red dots on the map. B. Rognoux valley
47
48 840 (Hofmann 2018). C. Arsine glacier (Schimmelpfennig *et al.* 2019). E. Argentièrè glacier (Protin
49
50 841 *et al.* 2019). F. Tsidjiore Nouve glacier (Schimmelpfennig *et al.* 2012). G. Belalp cirque
51
52 842 (Schindelwig *et al.* 2012). H. Steingletscher (Schimmelpfennig *et al.* 2014). I. Kromer valley
53
54 843 (Kerschner *et al.* 2006; Moran *et al.* 2016b). J. Kloster valley (Moran *et al.* 2016b). K. Falgin
55
56
57
58
59
60

1
2
3 844 glacier (Moran *et al.* 2016a). L. La Mare glacier (Baroni *et al.* 2017). M. Careser glacier (Baroni
4
5 845 *et al.* 2017). Vertical dashed lines delimit the YD/EH transition period between 12 and 10 ka.

6
7 846
8
9
10 847 Table 1. Characteristics and ^{10}Be measurement details of samples and blanks measured in this
11
12 848 study. Outliers are highlighted by (O). Results of the exposure ages are presented using both
13
14 849 the regional production rate (Claude *et al.* 2014) and the “Arctic” production rate (Young *et al.*
15
16 850 2013). Exposure ages are indicated with external uncertainties and internal uncertainties
17
18 851 (including the ^{10}Be production rate uncertainty) in parentheses. Mean landform ages of T1 and
19
20 852 T2 are indicated with standard deviations and total uncertainties (including the ^{10}Be production
21
22 853 rate uncertainty) in parentheses.
23
24
25

26 854

27
28 855

30 856 Supporting Information

31
32
33 857

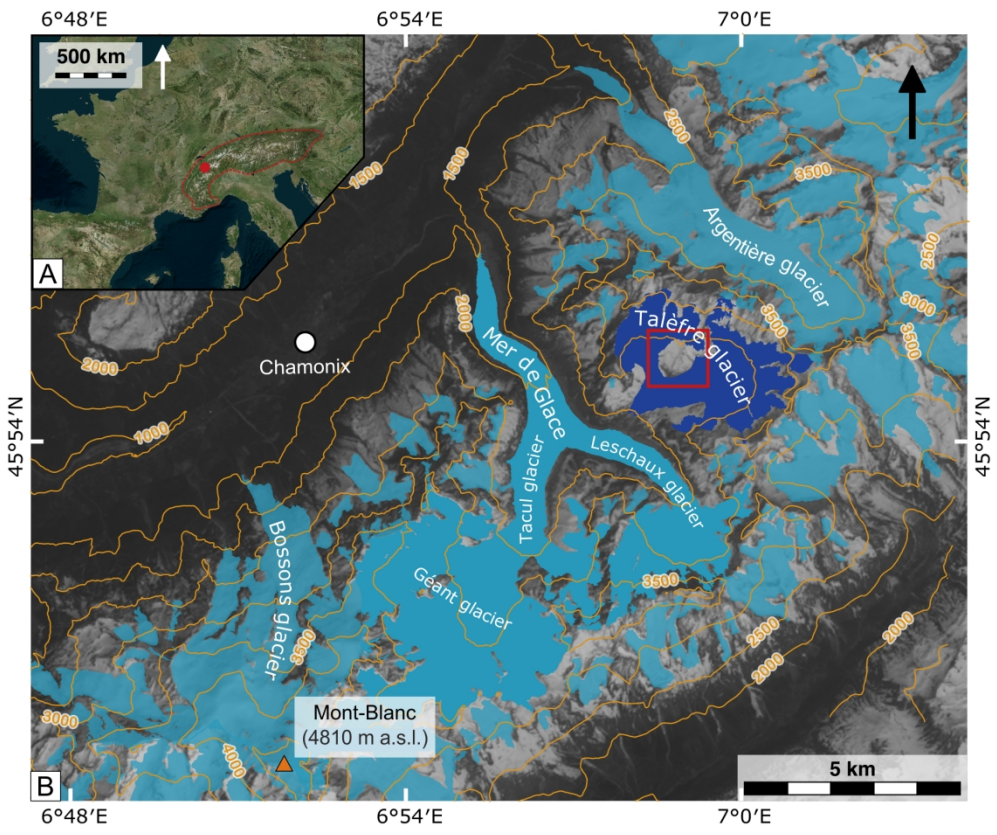
34
35
36 858 Fig. S1. Geographic characteristics of the Alpine glaciers selected for the comparison and
37
38 859 presented in Fig. 6 and comparison of ELA depression (relative to LIA). A. Wind rose
39
40 860 indicating the orientation of each glacier. B. Graph representing the present-day length of the
41
42 861 glaciers versus their maximum and minimum elevation. C. ELA depression (relative to LIA,
43
44 862 calculated with the AAR methods and 0.67 ratio) versus the age of the studied stadial. Letters
45
46 863 correspond to panels and locations in Fig. 6. As Rougnoux glacier (Hofmann 2018) has now
47
48 864 disappeared, it is not represented in A and B.
49

50
51
52 865

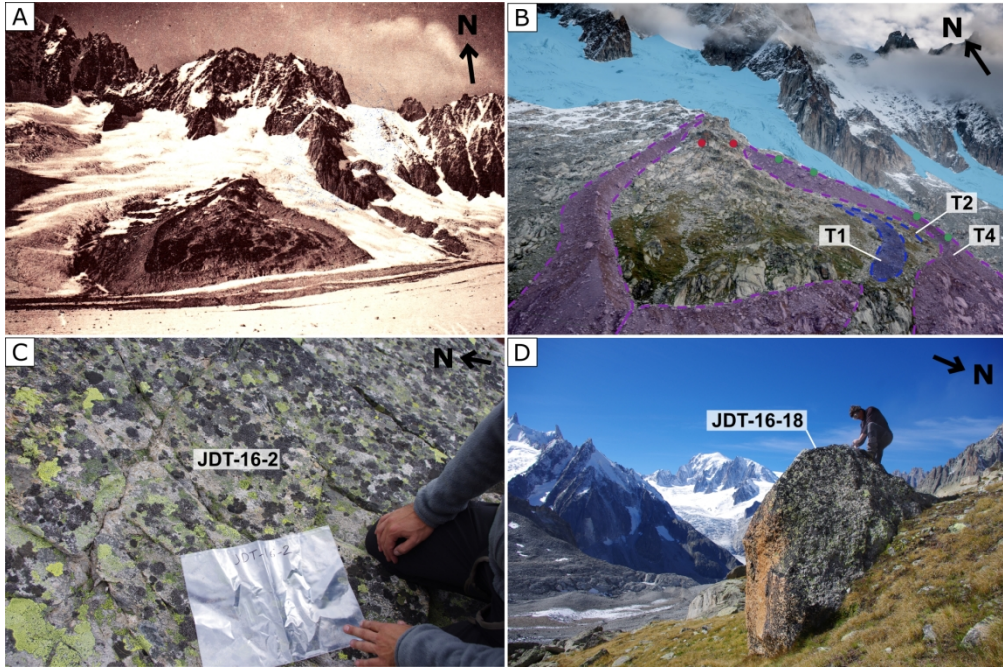
53
54 866 Table S1. ^{10}Be exposure ages from the previously published moraine records in the Alps that
55
56 867 were considered in the comparison with the moraine ages from Talèfre glacier and associated
57
58 868 ELA depressions (relative to LIA) when calculated in the original study. For comparison, all
59
60

1
2
3 869 ages were calculated using the same method as applied for the Talèfre samples (see “Age
4
5 870 calculations”). Outliers (O) were determined either based on original authors choice or on the
6
7 871 χ^2 test (2σ) as applied to the ages from Talèfre moraines. For samples from Cossart *et al.*
8
9 872 (2012), a sample thickness of 2 cm was assumed as this information is not given in the original
10
11 873 paper. When not specified by authors, we assumed a rock density of 2.7 g cm⁻³. Sites or
12
13 874 moraines that do not fulfill the selection criteria detailed in the main text are in italic while sites
14
15 875 that met the selection criteria for comparison are in bold. Capital letters in parentheses
16
17 876 correspond to panels and location in Fig. 6. ELA are calculated with the AAR method and a
18
19 877 0.67 ratio.
20
21
22
23
24
25
26
27
28
29
30
31
32
33
34
35
36
37
38
39
40
41
42
43
44
45
46
47
48
49
50
51
52
53
54
55
56
57
58
59
60

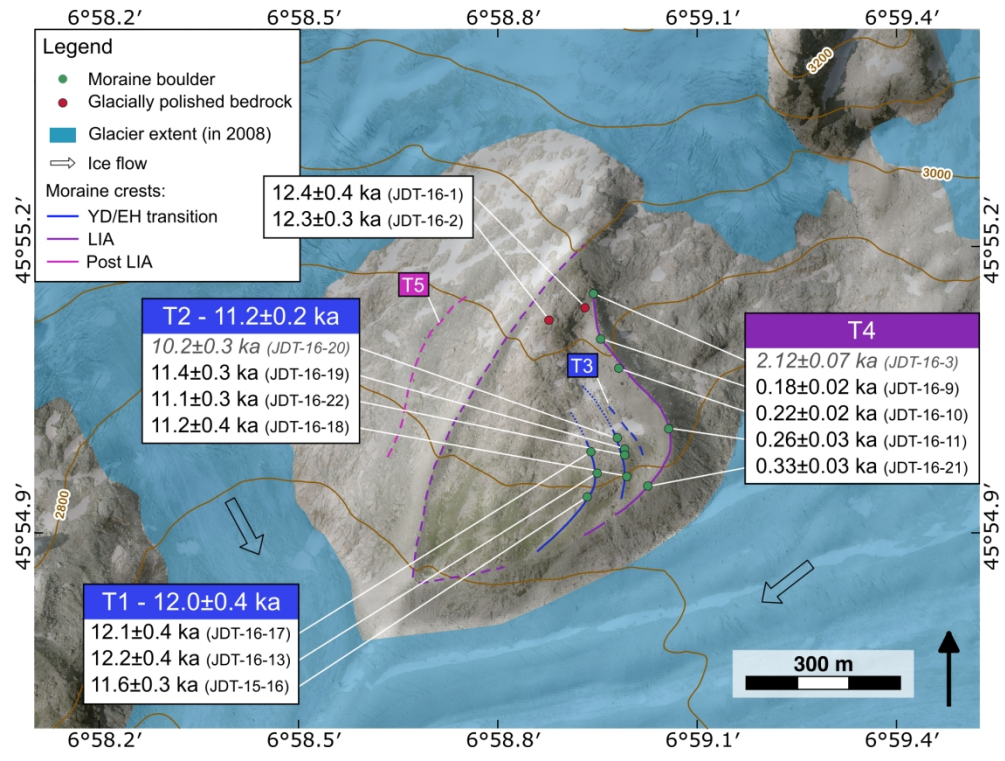
1
2
3
4
5
6
7
8
9
10
11
12
13
14
15
16
17
18
19
20
21
22
23
24
25
26
27
28
29
30
31
32
33
34
35
36
37
38
39
40
41
42
43
44
45
46
47
48
49
50
51
52
53
54
55
56
57
58
59
60



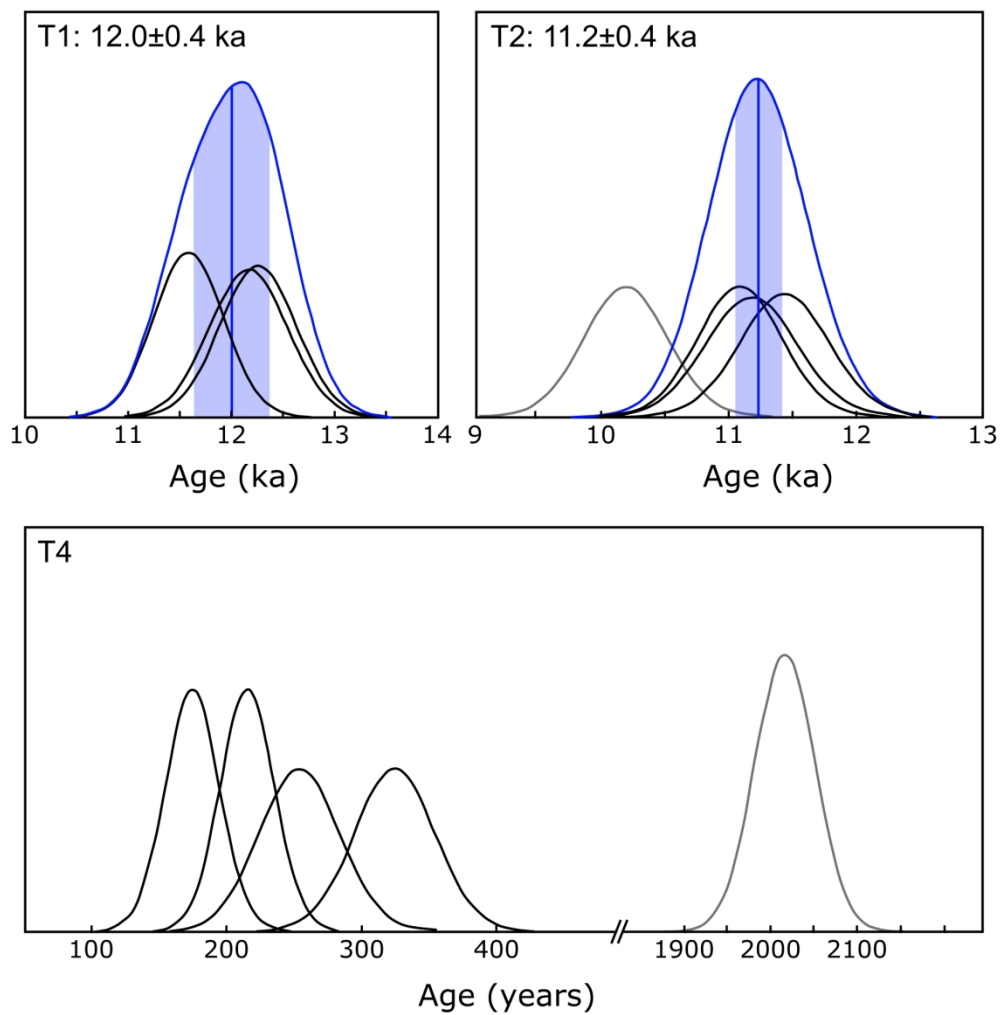
1
2
3
4
5
6
7
8
9
10
11
12
13
14
15
16
17
18
19
20
21
22
23
24
25
26
27
28
29
30
31
32
33
34
35
36
37
38
39
40
41
42
43
44
45
46
47
48
49
50
51
52
53
54
55
56
57
58
59
60



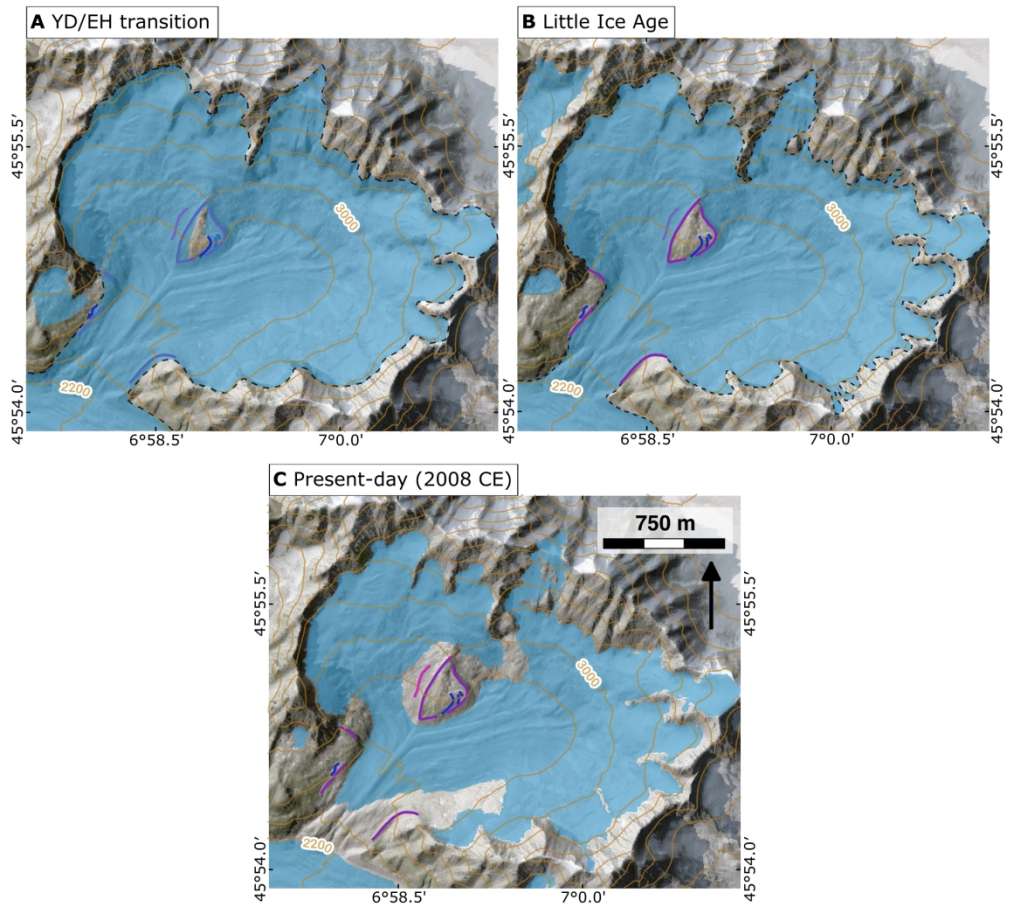
1
2
3
4
5
6
7
8
9
10
11
12
13
14
15
16
17
18
19
20
21
22
23
24
25
26
27
28
29
30
31
32
33
34
35
36
37
38
39
40
41
42
43
44
45
46
47
48
49
50
51
52
53
54
55
56
57
58
59
60

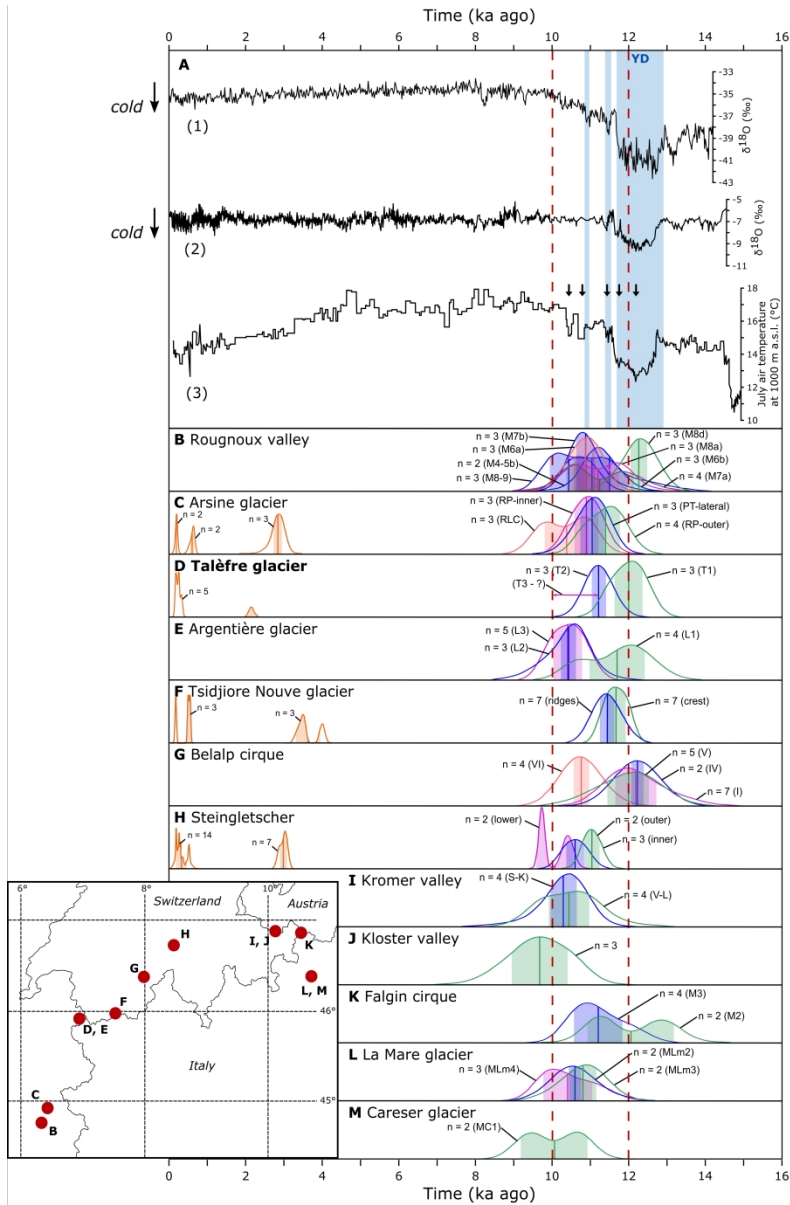


1
2
3
4
5
6
7
8
9
10
11
12
13
14
15
16
17
18
19
20
21
22
23
24
25
26
27
28
29
30
31
32
33
34
35
36
37
38
39
40
41
42
43
44
45
46
47
48
49
50
51
52
53
54
55
56
57
58
59
60



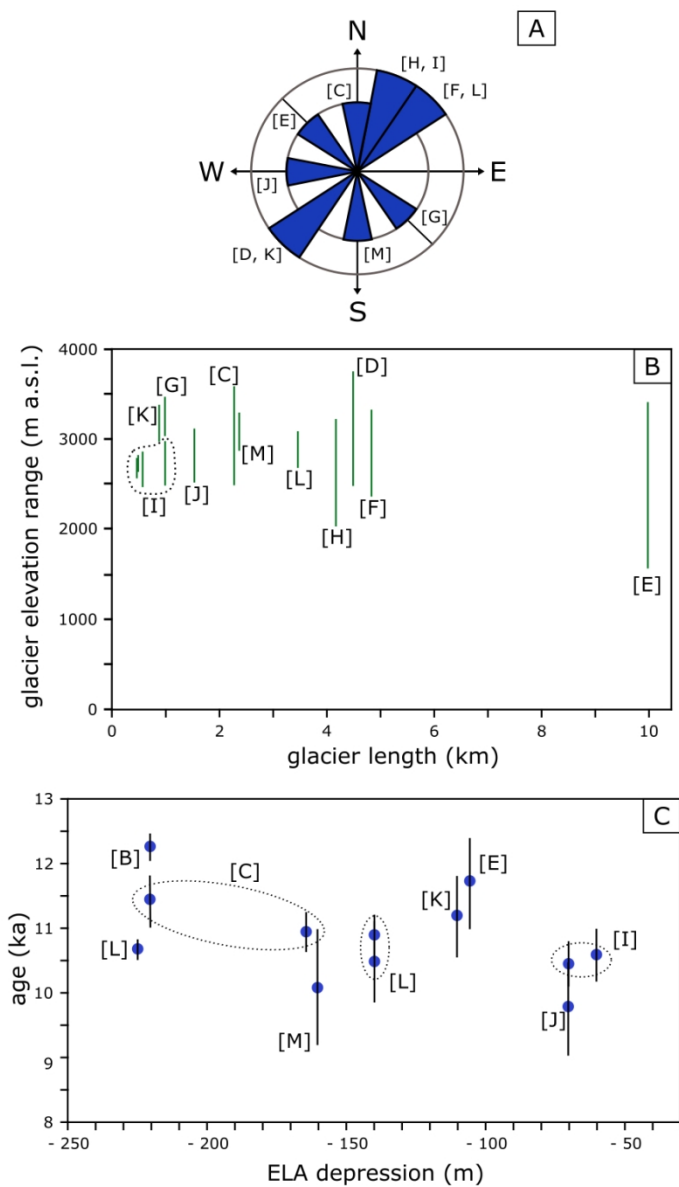
1
2
3
4
5
6
7
8
9
10
11
12
13
14
15
16
17
18
19
20
21
22
23
24
25
26
27
28
29
30
31
32
33
34
35
36
37
38
39
40
41
42
43
44
45
46
47
48
49
50
51
52
53
54
55
56
57
58
59
60





Sample name	Latitude (dd)	Longitude (dd)	Elevation (m a.s.l.)	Thickness (mm)	Shielding factor	Quartz weight (g)	Carrier (mg ⁹ Be)	Associated blank	¹⁰ Be/ ⁹ Be x10 ⁻¹⁴	¹⁰ Be (x10 ⁴ at g ⁻¹)	Regional PR		Arctic PR	
											¹⁰ Be age (ka)	1σ uncertainties (ka)	¹⁰ Be age (ka)	1σ uncertainties (ka)
Moraine samples														
T1											11.97±0.36 (0.46)		12.07±0.37 (0.83)	
JDT-16-17	45.91642	6.98233	2825	45	0.9063	24.67	0.3053	BLC-15Jan18	44.9±1.4	36.8±1.2	12.14	0.37 (0.47)	12.24	0.37 (0.82)
JDT-16-13	45.91604	6.98249	2817	27	0.9635	15.35	0.3072	BLC-15Jan18	30.13±0.93	39.8±1.2	12.21	0.36 (0.46)	12.32	0.37 (0.83)
JDT-16-16	45.91564	6.98224	2798	22	0.9635	28.65	0.3078	BLC-15Jan18	52.3±1.6	37.3±1.2	11.56	0.34 (0.42)	11.65	0.35 (0.77)
T2											11.21±0.17 (0.32)		11.30±0.18 (0.71)	
JDT-16-20 (O)	45.91667	6.98301	2835	42	0.9638	26.58	0.3071	BLC-15Jan18	42.7±1.4	32.7±1.1	10.15	0.32 (0.40)	10.24	0.32 (0.68)
JDT-16-19	45.91647	6.98318	2827	25	0.9638	21.49	0.3070	BLC-15Jan18	39.5±1.3	37.4±1.2	11.40	0.34 (0.43)	11.50	0.35 (0.76)
JDT-16-22	45.91636	6.98320	2824	24	0.9638	32.44	0.3069	BLC-15Jan18	57.6±1.8	36.2±1.1	11.07	0.33 (0.41)	11.16	0.33 (0.73)
JDT-16-18	45.91599	6.98324	2805	35	0.9527	20.18	0.3083	BLC-15Jan18	34.9±1.2	35.3±1.2	11.15	0.35 (0.44)	11.24	0.36 (0.75)
T3														
JDT-16-3 (O)	45.91918	6.98241	2951	20	0.9677	37.83	0.3048	BLC-08Dec17	13.43±0.42	7.05±0.23	2.12	0.07 (0.09)	2.15	0.07 (0.19)
JDT-16-9	45.91840	6.98260	2923	38	0.9625	31.65	0.3033	BLC-08Dec17	1.33±0.11	0.64±0.08	0.18	0.02 (0.02)	0.18	0.02 (0.02)
JDT-16-10	45.91788	6.98305	2903	28	0.9625	31.26	0.3017	BLC-08Dec17	1.56±0.11	0.78±0.08	0.22	0.02 (0.02)	0.22	0.03 (0.03)
JDT-16-11	45.91683	6.98430	2842	26	0.9434	36.61	0.3063	BLC-08Dec17	1.88±1.20	0.86±0.07	0.26	0.03 (0.03)	0.26	0.02 (0.03)
JDT-16-21	45.91583	6.98377	2796	22	0.9623	33.60	0.3010	BLC-08Dec17	2.16±0.12	1.09±0.08	0.33	0.03 (0.03)	0.33	0.03 (0.03)
Bedrock samples														
JDT-16-1	45.91873	6.98128	2950	32	0.9667	20.09	0.3015	BLC-08Dec17	44.2±1.4	44.0±1.4	12.43	0.38 (0.48)	12.54	0.39 (0.85)
JDT-16-2	45.91894	6.98219	2943	26	0.9677	17.83	0.3048	BLC-08Dec17	38.6±1.1	43.7±1.2	12.31	0.33 (0.44)	12.42	0.34 (0.81)
Blanks														
Blank name	Carrier (mg ⁹ Be)		¹⁰ Be/ ⁹ Be x10 ⁻¹⁴		Number of ¹⁰ Be atoms (x10 ⁴ at)									
BLC-8Dec17	0.3040		0.338±0.049		6.9±1.0									
BLC-15Jan18	0.3075		0.348±0.050		7.2±1.0									

1
2
3
4
5
6
7
8
9
10
11
12
13
14
15
16
17
18
19
20
21
22
23
24
25
26
27
28
29
30
31
32
33
34
35
36
37
38
39
40
41
42
43
44
45
46
47
48
49
50
51
52
53
54
55
56
57
58
59
60



Moraine and sample name	Regional PR			Arctic PR			Δ ELA compare to LIA (m)
	Recalculated ^{10}Be age (ka)	1σ uncertainty (ka)	Moraine age (ka)	Recalculated ^{10}Be age (ka)	1σ uncertainty (ka)	Moraine age (ka)	
Rougnoix Valley (B) (Hofmann 2018)							
VdR M8d			12.3±0.2			12.4±0.2	-220
VdR-26	12.43	0.42 (0.51)		12.53	0.42 (0.86)		
VdR-27	12.34	0.42 (0.50)		12.44	0.42 (0.86)		
VdR-28	12.01	0.53 (0.59)		12.11	0.53 (0.90)		
VdR M7a			11.3±0.9			11.3±0.9	
VdR-23	10.38	0.42 (0.47)		10.45	0.42 (0.74)		
VdR-24	12.25	0.56 (0.62)		12.35	0.56 (0.93)		
VdR-25-1	11.76	0.40 (0.48)		11.85	0.40 (0.81)		
VdR-25-2	10.66	0.32 (0.40)		10.74	0.32 (0.70)		
VdR M4-5b			11.5±0.5			11.6±0.5	
VdR-10	11.17	0.37 (0.45)		11.27	0.37 (0.75)		
VdR-11	11.83	0.92 (0.95)		11.93	0.92 (1.16)		
VdR-12 (O)	7.41	0.38 (0.41)		7.46	0.38 (0.56)		
VdR M8a			11.2±0.6			11.3±0.6	
VdR-16	11.74	0.38 (0.47)		11.83	0.38 (0.80)		
VdR-17	10.64	0.40 (0.46)		10.71	0.40 (0.74)		
VdR-18	11.21	1.19 (1.21)		11.30	1.19 (1.36)		
VdR M6b			11.0±0.5			11.1±0.5	
VdR-7	11.42	0.40 (0.48)		11.50	0.40 (0.78)		
VdR-8	11.17	0.66 (0.70)		11.25	0.66 (0.93)		
VdR-9	10.53	0.36 (0.42)		10.62	0.36 (0.71)		
VdR M6a			10.9±0.4			11.0±0.4	
VdR-13	1.38	0.12 (0.13)		1.39	0.12 (0.16)		
VdR-14	11.12	0.34 (0.42)		11.21	0.34 (0.74)		
VdR-15	10.62	0.38 (0.45)		10.69	0.38 (0.73)		
VdR M7b			10.9±0.2			11.0±0.2	
VdR-4	10.66	0.36 (0.43)		10.74	0.36 (0.73)		
VdR-5	11.13	0.55 (0.60)		11.22	0.55 (0.86)		
VdR-6	10.83	0.33 (0.41)		10.92	0.33 (0.71)		
VdR M8-9			10.4±0.5			10.5±0.5	
VdR-1	10.97	0.35 (0.43)		11.06	0.35 (0.73)		
VdR-2	10.35	0.43 (0.49)		10.43	0.43 (0.75)		
VdR-3	10.00	0.36 (0.42)		10.07	0.36 (0.69)		
Arsine Glacier (C) (Schimmelpfennig <i>et al.</i> 2019)							
Frontal moraine			11.4±0.4				-220
Petit Tabuc lateral moraine			11.0±0.3			11.1±0.3	
Rif de la Planche frontale moraine			10.9±0.3			11.0±0.3	-164
Right lateral complex			10.4±0.6			10.5±0.6	
Piano del Praiet (Federici <i>et al.</i> 2008)							
PDP moraine			14.5±0.9			14.6±0.9	
PDP1	15.27	0.61 (1.32)		15.42	0.61 (1.08)		
PDP2	15.00	0.83 (1.44)		15.16	0.83 (1.21)		
PDP3	14.35	0.58 (1.24)		14.52	0.58 (1.02)		
PDP4	13.03	0.59 (1.18)		13.45	0.59 (0.99)		
Argentière Glacier (E) (Protin <i>et al.</i> 2019)							
L1			11.7±0.7			10.8±0.7	-105
ARG-16-9	12.21	0.58 (0.64)		12.31	0.58 (0.94)		
ARG-16-10 (O)	10.10	0.65 (0.68)		10.18	0.65 (0.88)		
ARG-16-11	10.63	0.42 (0.48)		10.70	0.42 (0.75)		
ARG-16-12	11.88	0.68 (0.73)		11.97	0.68 (0.99)		
ARG-16-13	11.93	0.55 (0.61)		12.03	0.55 (0.91)		

1							
2							
3	L2			10.4±0.2			10.5±0.2
4	ARG-16-1	10.28	0.66 (0.70)		10.36	0.66 (0.90)	
5	ARG-16-2	10.39	0.66 (0.70)		10.47	0.66 (0.90)	
6	ARG-15-11	10.65	0.32 (0.40)		10.73	0.32 (0.70)	
7	L3			10.4±0.4			10.5±0.4
8	ARG-16-3	10.61	0.33 (0.41)		10.68	0.33 (0.70)	
9	ARG-16-4	10.52	0.32 (0.40)		10.60	0.32 (0.70)	
10	ARG-15-12	10.87	0.33 (0.40)		10.96	0.33 (0.72)	
11	ARG-16-5 (O)	17.42	1.51 (1.55)		17.56	1.51 (1.82)	
12	ARG-16-6	10.04	0.30 (0.38)		10.11	0.31 (0.67)	
13	ARG-16-7	10.01	0.34 (0.41)		10.10	0.34 (0.69)	
14							
15	<i>Romanche Valley (Chenet et al. 2016)</i>						
16	M7			12.5±0.8			12.5±0.9
17	RO-20	13.04	0.67 (0.73)		13.16	0.67 (1.04)	
18	RO-21	11.86	0.58 (0.63)		11.93	0.58 (0.92)	
19	RO-22 (O)	16.15	1.86 (1.88)		16.27	1.86 (2.09)	
20	RO-23 (O)	7.72	0.61 (0.64)		7.79	0.61 (0.76)	
21	RO-24 (O)	12.98	3.62 (3.61)		13.09	3.62 (3.71)	
22	M6			11.9±0.8			12.0±0.8
23	RO-15	12.29	0.93 (0.96)		12.38	0.93 (1.19)	
24	RO-16	10.30	0.89 (0.92)		10.39	0.89 (1.08)	
25	RO-17	11.72	0.63 (0.68)		11.81	0.63 (0.95)	
26	RO-18	13.10	0.69 (0.76)		13.23	0.69 (1.05)	
27	RO-19 (O)	2.08	0.41 (0.41)		2.1	0.41 (0.43)	
28							
29	<i>Clarée Valley (Cossart et al. 2012)</i>						
30	Stage 2 moraine			12.7±1.1			12.8±1.1
31	CLA_08_13a	11.43	0.85 (0.88)		11.51	0.85 (1.09)	
32	CLA_08_13b	13.21	0.64 (0.71)		13.33	0.64 (1.02)	
33	CLA_08_14	13.51	0.93 (0.98)		13.61	0.93 (1.23)	
34	Stage 3 moraine			11.4±1.2			11.5±1.2
35	CLA_08_01	12.15	0.42 (0.50)		12.25	0.42 (0.84)	
36	CLA_08_02a	12.63	0.74 (0.80)		12.74	0.74 (1.06)	
37	CLA_08_02b (O)	14.09	0.69 (0.76)		14.23	0.69 (1.08)	
38	CLA_08_03	11.78	0.54 (0.59)		11.87	0.54 (0.89)	
39	CLA_08_04	10.74	0.61 (0.65)		10.82	0.61 (0.88)	
40	CLA_08_05	12.51	0.81 (0.85)		12.60	0.81 (1.10)	
41	CLA_08_06	10.12	3.19 (3.17)		10.20	3.19 (3.24)	
42	CLA_08_10	9.83	3.79 (3.76)		9.92	3.79 (3.83)	
43							
44	<i>Tsidjiore Nouve Galcier (F) (Schimmelpfennig et al. 2012)</i>						
45	Crest			11.7±0.2			11.8±0.2
46	ARO-4	11.94	0.18 (0.33)		12.04	0.18 (0.74)	
47	ARO-1	11.90	0.21 (0.35)		12.01	0.21 (0.75)	
48	ARO-6	11.87	0.24 (0.36)		11.98	0.24 (0.76)	
49	ARO-55	11.63	0.18 (0.32)		11.73	0.18 (0.72)	
50	ARO-5	11.58	0.21 (0.33)		11.67	0.21 (0.72)	
51	ARO-52	11.39	0.20 (0.33)		11.50	0.20 (0.70)	
52	ARO-59	11.34	0.20 (0.33)		11.44	0.20 (0.70)	
53	ARO-3 (O)	11.20	0.19 (0.32)		11.29	0.19 (0.69)	
54	ARO-56 (O)	11.05	0.19 (0.32)		11.14	0.19 (0.68)	
55	ARO-2 (O)	10.96	0.19 (0.31)		11.05	0.19 (0.67)	
56	Recessional ridges			11.4±0.2			11.5±0.2
57	ARO-21_2010Apr	11.72	0.28 (0.38)		11.82	0.28 (0.75)	
58	ARO-21	11.62	0.23 (0.34)		11.72	0.23 (0.73)	
59	ARO-22	11.48	0.26 (0.37)		11.58	0.26 (0.73)	
60	ARO-21-re	11.39	0.20 (0.33)		11.48	0.20 (0.70)	
	ARO-18	11.32	0.31 (0.40)		11.42	0.31 (0.74)	

1						
2						
3	ARO-8	11.3	0.20 (0.32)	11.41	0.20 (0.70)	
4	ARO-16	11.2	0.19 (0.32)	11.29	0.19 (0.69)	
5	ARO-7 (O)	12.28	0.20 (0.35)	12.39	0.20 (0.77)	
6	ARO-15 (O)	10.99	0.27 (0.36)	11.08	0.27 (0.70)	
7						
8	Belalp Cirque (G) (Schindelwig <i>et al.</i> 2012)					
9	Moraine I			12.0±0.6		12.1±0.6
10	VBA-3 (O)	15.08	0.57 (0.66)	15.17	0.57 (1.05)	
11	VBA-22	12.49	0.57 (0.63)	12.58	0.57 (0.94)	
12	VBA-23	12.57	0.82 (0.87)	12.65	0.82 (1.11)	
13	VBA-24	11.95	0.82 (0.86)	12.02	0.82 (1.09)	
14	VBA-25	12.04	0.66 (0.71)	12.11	0.66 (0.98)	
15	VBA-26	11.09	0.71 (0.75)	11.16	0.71 (0.97)	
16	Moraine IV			12.3±0.2		12.4±0.2
17	VBA-6	12.18	0.61 (0.66)	12.25	0.61 (0.96)	
18	VBA-15 (O)	9.82	0.94 (0.97)	9.88	0.94 (1.11)	
19	VBA-16	12.43	0.65 (0.70)	12.51	0.65 (0.99)	
20	Moraine V			12.2±0.6		12.3±0.6
21	VBA-1	13.36	0.68 (0.74)	13.44	0.68 (1.05)	
22	VBA-2	11.77	0.57 (0.63)	11.86	0.57 (0.90)	
23	VBA-4 (O)	10.32	0.64 (0.68)	10.38	0.64 (0.88)	
24	VBA-5	11.78	0.54 (0.60)	11.85	0.54 (0.88)	
25	VBA-11	12.16	0.66 (0.72)	12.23	0.66 (0.99)	
26	VBA-12	12.78	0.71 (0.77)	12.85	0.71 (1.05)	
27	VBA-13	11.85	0.64 (0.70)	11.92	0.64 (0.95)	
28	VBA-14	12.02	0.61 (0.66)	12.1	0.61 (0.95)	
29	Moraine VI			10.7±0.1		10.8±0.1
30	VBA-17	10.52	0.47 (0.53)	10.58	0.47 (0.78)	
31	VBA-18	10.53	0.55 (0.60)	10.59	0.55 (0.83)	
32	VBA-19	10.74	0.51 (0.57)	10.81	0.51 (0.82)	
33	VBA-20	10.96	0.61 (0.66)	11.03	0.61 (0.90)	
34						
35	<i>Great Aletsch</i> (Schindelwig <i>et al.</i> 2012)					
36				12.6±0.8		12.7±0.8
37	VBA-7	13.14	0.74 (0.80)	13.24	0.74 (1.08)	
38	VBA-8	13.36	0.54 (0.62)	13.46	0.54 (0.97)	
39	VBA-9	11.83	0.97 (1.00)	11.93	0.97 (1.20)	
40	VBA-10	12.07	0.74 (0.79)	12.14	0.74 (1.04)	
41						
42	<i>GREAT ALETSCHE</i> (Kelly <i>et al.</i> , 2004)					
43				12.3±0.2		12.4±0.2
44	AG-1	12.45	0.51 (0.59)	12.54	0.51 (0.91)	
45	AG-2	11.69	0.81 (0.84)	11.78	0.81 (1.07)	
46	AG-4	13.16	0.48 (0.99)	12.77	0.48 (0.91)	
47	AG-5	12.09	0.70 (0.82)	13.49	0.70 (1.07)	
48						
49	Steingletscher (H) (Schimmelpfennig <i>et al.</i> 2014)					
50	Outer moraine			11.0±0.2		11.1±0.2
51	STEI-27	11.18	0.20 (0.32)	11.26	0.20 (0.69)	
52	STEI-11	10.91	0.19 (0.31)	10.99	0.19 (0.67)	
53	Inner moraine			10.6±0.2		10.7±0.2
54	STEI-8	10.81	0.26 (0.35)	10.90	0.26 (0.69)	
55	STEI-9	10.65	0.29 (0.37)	10.73	0.29 (0.69)	
56	STEI-10	10.36	0.23 (0.33)	10.44	0.23 (0.66)	
57	Lower moraine			10.1±0.5		10.2±0.5
58	STEI-19	10.43	0.15 (0.28)	10.51	0.15 (0.64)	
59	STEI-20	9.75	0.08 (0.24)	9.82	0.08 (0.59)	
60	STEI-21 (O)	8.72	0.08 (0.22)	8.78	0.08 (0.53)	

Val Viola (Hormes *et al.* 2008)

moraine				12.5±0.5			12.6±0.5	
	VVm4	12.14	0.65 (0.70)		12.23	0.65 (0.70)		
	VVm5	12.8	0.04 (0.30)		12.92	0.04 (0.78)		

Ferwall Site (Ivy-Ochs *et al.* 2006)

Schönferwall				13.4±0.4			13.6±0.4	
	F1	13.38	1.01 (1.05)		13.49	1.01 (1.29)		
	F2	14	0.99 (1.04)		14.12	0.99 (1.31)		
	F3	13.02	0.65 (0.71)		13.12	0.65 (1.02)		
	F4b	13.38	0.75 (0.81)		13.47	0.75 (1.10)		
Kartell				12.1±0.4			12.2±0.4	
	K1	12.32	0.95 (1.00)		12.44	0.96 (1.21)		
	K2	11.58	0.59 (0.64)		11.7	0.59 (0.91)		
	K3a	12.3	1.04 (1.08)		12.42	1.04 (1.28)		

Kromer Valley (I) (Kerschner *et al.* 2006; Moran *et al.* 2016b)

Verhulf-Litzer moraine system				10.6±0.4			10.6±0.4	-60
	KR-1	10.67	0.49 (0.54)		10.75	0.49 (0.80)		
	KR-2	11.12	0.49 (0.56)		11.2	0.50 (0.83)		
	KR-203	10.68	1.27 (1.28)		10.76	1.27 (1.42)		
	KR-303	9.86	0.41 (0.46)		9.94	0.41 (0.71)		
	KR-205 (O)	9.32	0.47 (0.51)		9.39	0.47 (0.73)		
	KR-305 (O)	8.27	0.35 (0.40)		8.34	0.35 (0.60)		
Scheizer-Kromer moraine system				10.4±0.3			10.5±0.3	-70
	KR-3	10.58	0.50 (0.55)		10.66	0.50 (0.81)		
	KR-4	10.35	0.45 (0.50)		10.43	0.45 (0.76)		
	KR-5	10.82	0.41 (0.48)		10.9	0.41 (0.76)		
	KR-201	10.02	0.92 (0.95)		10.11	0.92 (1.10)		

Kloster Valley (J) (Moran *et al.* 2016b)

Kloster valley moraine system				9.8±0.7			9.8±0.7	-70
	KL-1	10.51	0.51 (0.56)		10.58	0.51 (0.81)		
	KL-2A	9.07	0.65 (0.68)		9.14	0.65 (0.85)		
	KL-2B	9.7	0.49 (0.54)		9.78	0.49 (0.76)		

Falgin Cirque (H) (Moran *et al.* 2016a)

M1				13.0±0.5			13.1±0.5	
	LT-9	12.96	0.51 (0.59)		13.08	0.51 (0.94)		
M2				12.1±1.1			12.2±1.1	
	LT-6	11.27	0.43 (0.49)		11.37	0.43 (0.79)		
	LT-7	12.86	0.50 (0.59)		12.99	0.50 (0.93)		
M3				11.2±0.5			11.3±0.6	-110
	LT-2	12.01	0.46 (0.54)		12.11	0.46 (0.86)		
	LT-3	11.29	0.43 (0.50)		11.38	0.43 (0.80)		
	LT-4	10.89	0.41 (0.48)		10.98	0.41 (0.76)		
	LT-5	10.56	0.40 (0.47)		10.64	0.40 (0.74)		

La Mare GalcierR (I) (Baroni *et al.* 2017)

MLm1				12.2±0.4			12.3±0.4	-225
	LAM 13.3	12.21	0.41 (0.50)		12.32	0.41 (0.85)		
MLm2				10.7±0.2			10.8±0.2	-225
	LAM 14.1	10.79	0.83 (0.86)		10.87	0.83 (1.05)		
	LAM 14.2	10.56	0.52 (0.57)		10.64	0.52 (0.81)		
MLm3				10.9±0.3			11.0±0.3	-140
	LAM 13.1	10.63	0.63 (0.67)		10.72	0.63 (0.89)		
	LAM 13.2	11.12	0.51 (0.56)		11.2	0.51 (0.83)		

1								
2								
3	MLm4			10.5±0.6			10.6±0.6	-140
4		LAM 13.4	11.17	0.51 (0.57)		11.26	0.51 (0.84)	
5		LAM 13.5	10.35	0.48 (0.54)		10.43	0.48 (0.78)	
6		LAM 13.6	9.92	0.40 (0.45)		10	0.40 (0.71)	
7								
8	Careser Glacier (J) (Baroni <i>et al.</i> 2017)							
9	MC2			10.1±0.4			10.2±0.4	-180
10		POVE 3	10.08	0.42 (0.48)		10.16	0.42 (0.74)	
11	MCI			10.1±0.9			10.1±0.9	-160
12		POVE 1	10.71	0.42 (0.48)		10.73	0.42 (0.76)	
13		POVE 2	9.42	0.43 (0.48)		9.51	0.43 (0.71)	
14								
15								
16								
17								
18								
19								
20								
21								
22								
23								
24								
25								
26								
27								
28								
29								
30								
31								
32								
33								
34								
35								
36								
37								
38								
39								
40								
41								
42								
43								
44								
45								
46								
47								
48								
49								
50								
51								
52								
53								
54								
55								
56								
57								
58								
59								
60								

For Review Only